Holography : Recording/Reconstruction

Pascal PICART

21.05.2024

Table des matières

I.Présentation

Module :

Interference and Diffraction

Auteur(s) :

Pascal PICART[1] - ENSIM – Le Mans Université

Résumé :

The course is about holographic principle from notions linked to diffraction and interferences. The formation of images is analysed for analogical and digital holography. Digital holograms reconstruction is tackled by introducing the different reconstruction strategies. The case study is about the digital holograms realization and the exercises part gets onto combining holographic relationships.

Mots-clés :

Holography, diffraction, Interferences, Fresnel transform, Numerical hologram

Pré-requis :

Diffraction, Interferences, Signal treatment, discrete Fourier transform, convolution

Objectif(s) pédagogique(s) :

The objective is to know the analogical and digital holographic principle. It is also being able to introduce a digital holographic interferometer and be able to treat holograms digitally.

Plan du cours :

- Introduction
- Analogue Holography
- Digital Holography
- Conclusion

Conception & production :

Le Mans Université

Licence :

1 - pascal.picart@univ-lemans.fr
2 - http://www.gnu.org/licenses/fdl.txt

II.Cours

Holography was invented in 1947 by the Hungarian physicist Dennis Gabor [1 [A New Microscopic Principle]] while he was carrying out research on electronic microscopy. D.Gabor received the Nobel Prize for Physics in 1971 for this invention. However, it wasn't until 1962 [2 [Reconstructed Wavefront and Communication Theory]] and the invention of the first lasers that this technique had a concrete use.

Holography comprises the successful combination of interferences and diffraction. The interferences encode the amplitude and the contours of a three-dimensional object and the diffraction acts as a decoder which reconstructs a wave which seems to be formed from the previously illuminated object. This encoding as the etymology of the word 'holography' would suggest ("holo" = whole, "graph" = writing/drawing), contains all the necessary information: the optic phase and therefore the depth and contours of the object.

In practice, the analogical process that has been known about for 40 years can be broken down into 3 stages :

- The first stage pertains to the reading of the interferences on a photosensitive plate.
- The second stage involves a chemical process in order to develop the plate and typical lasts for a good quarter of an hour for silver photo plates.
- The last stage is the process of physically reconstructing the object wave during which a laser is diffracted onto the sinusoidal network encoded within the photosensitive plate.

Considering the restraints related to the processing of holograms (an essential stage in the development process), which makes it difficult to use them in industry (for example in quality control on a production line), it was considered as early as 1972 [3 [Reconstruction of a Hologram With a Computer]] to replace the silver photo plate with a matrix of holographic discrete values. The idea was to replace the analogue recording/decoding of the object with a digital recording/decoding process simulating a diffraction onto a digital network made from the recorded image. Holography had gone "digital".

Work presented by Konrod et al. in 1972 was the first attempt at reconstruction by calculation of an object encoded in a hologram. At the time, it took 6 hours of calculation to reconstruct a field of pixels, using the Minsk-22 computer. The discrete values were obtained from a plate hologram by 64 bit digitization with a scanner. However, it wasn't until the 1990s that matrix detector-based digital holography became a reality.[4 [Direct Recording of Holograms by a CCD Target and Numerical Reconstruction]]

Indeed, important evolutions have taken place in two areas of the technology :

- From that time period on, microtechnological processes have enabled detector matrices with sufficiently miniaturized pixels to be obtained in order to respond to the Shannon criteria concerning the discretisation of the spatial distribution of light.
- The computerised processing of images became accessible thanks, in the most part, to the notable improvement in the performance of microprocessors, particularly in their central processing unit (CPU) as well as in their virtual memory space.

This course will first tackle so-called "**analogue**" holography before moving on to so-called "**digital**" holography. These two sections will deal with the recording of a hologram as well as with the reconstruction of the encoded object, considering the types of photosensitive plate which are used. The case study section will introduce the results of experiments into the "digital" reconstruction of holograms. The exercise section will put forward several sets of problems linked to the experimental implementation of holography.

1. Analogue Holography

Holography is closely linked to the undulatory nature of light. Indeed the latter is explained using the principles of diffraction and interferences.

Holograms are defined by the interference between two waves, the "**object wave**" and the "**reference wave**". A misuse of language has meant that holograms are often defined as being the stereoscopic image seen by the observer. In reality; the hologram is defined as being the interferential pattern of the combination of the two previously mentioned waves.

This pattern contains the information, stored as complex amplitude, of the studied object field; thus, it is possible to reconstruct the object field in its entirety, both amplitude and phase, from the holographic plate. It is the phase information which makes it possible to reconstruct the contours of the object, and to recreate the parallax. The reconstruction of the recorded image is linked to the occurrence of diffraction.

1.1. Recording a Hologram

a) Diffraction Principle

Let's consider a stretched object lit by a monochromatic light wave, situated in the dimension z_s with regards to the recording plane. This object diffracts a wave towards the observation plane situated at the distance of $d_0 = |z_0|$. The surface of the illuminated object generates a wave front that we observe as :

$$A(x, y) = A_0 \exp(j \psi_0(x, y))$$

The amplitude describes the reflectivity of the object and the phase describes the surface appearance and its depth. Taking into account the results of the diffraction theory within the limits of the Fresnel conditions, the diffracted field at the dimension d_0 is expressed by an integral as follows :

$$O(x', y', d_0) = -\frac{j \exp(2 j \pi d_0/\lambda)}{\lambda d_0} \exp\left(\frac{j \pi}{\lambda d_0}(x'^2 + y'^2)\right)$$
$$\times \int_{-\infty}^{+\infty}\int_{-\infty}^{+\infty} A(x, y) \exp\left(\frac{j \pi}{\lambda d_0}(x^2 + y^2)\right) \exp\left(-\frac{2 j \pi}{\lambda d_0}(x x' + y y')\right) dxdy$$

Figure 1 illustrates the geometry of the diffraction as well as the variables which are used.

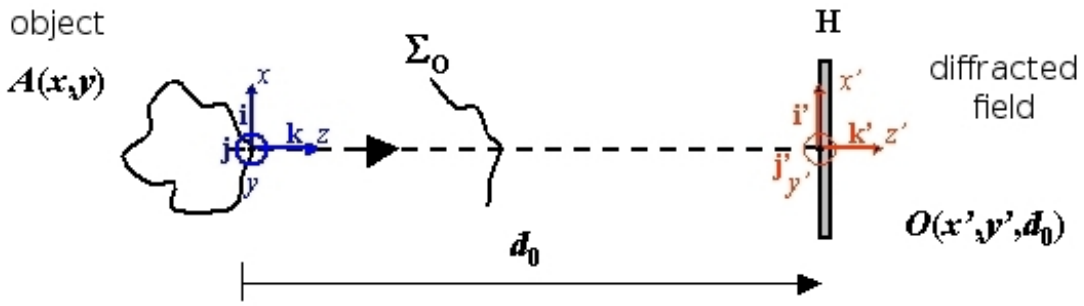

Figure 1 : Diffraction in a free field and notations

The diffracted field is equal to the Fresnel transformation of the distribution of amplitude on the abject surface. In the observation plane, this wave could equally be notated by the following simple equation :

$$O(x',y') = a_O(x',y') \exp\left(j\,\varphi_O(x',y')\right)$$

Where a_O is the complex amplitude modulus and φ_O is the phase. Given that the object is a natural diffusant, because it does not have a polished or light-reflecting surface, the diffracted field at the distance dimension d_0 is a speckle pattern. That is to say that the distribution of amplitude and phase in the observation plane is unpredictable. The phase φ_0 is therefore unpredictable because of the coarse nature of the object's surface and we can observe that it is consistent around $[-\pi, +\pi]$.

b) Interferometric Principles

The process used in holography requires interferences to be formed in order to encode the information. Thus, the wave which is diffracted by the object is coherently mixed with a reference wave in the observation plane. The interferences between the two waves require the use of a temporally and spatially consistent source (typically a laser) and result in an intensity pattern which represents the modulus squared of the sum of the two complex amplitudes. Figure 2 illustrates the geometry of the interference scheme.

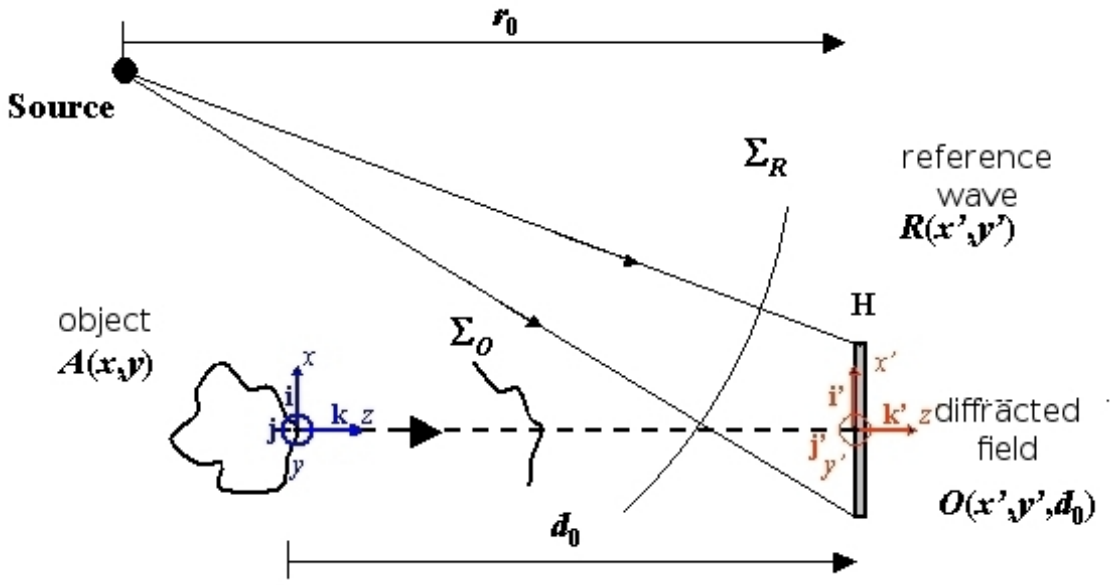

Figure 2 : Interferences between the diffractec wave and the reference wave

Thus, note that R is the complex amplitude of the reference wave front in the recording plane :

$$R(x',y') = a_R(x',y') \exp\left(j\,\varphi_R(x',y')\right)$$

Where a_R is the modulus of the complex amplitude and φ_R is the phase of the wave front. The reference wave generally comes from a source pinhole : it is therefore spherically divergent and in oblique incidence on the recording material. If we take the coordinates of the source point as (x_s, y_s, z_s) in the set of reference coordinates of the holographic plane $(z_s < 0)$, the optic phase of the reference wave is written in Fresnel's approximations as follows :

$$\varphi_R(x',y') = -\frac{\pi}{\lambda\, z_s}\left[(x'-x_s)^2 + (y'-y_s)^2\right]$$

Its optic phase could also be written in the form :

$$\varphi_R(x',y') = 2\pi\left(u_R x' + v_R y'\right) + \frac{\pi}{\lambda r_0}\left(x'^2 + y'^2\right) + \varphi_s$$

Where (u_R, v_R) are the information carrying spatial frequencies, $r_0 = |z_s|$ is the radius of the curvature of the wave and φ_s is a constant. Generally, it turns out that the wave is uniform, that is to say that $a_R(x', y') = C^{te}$. The total illumination received by the holographic materials is written :

$$H = |R|^2 + |O|^2 + R^* O + R O^*$$

This equation could also be written under the form :

$$H = a_R^2 + a_O^2 + 2\, a_R\, a_O \cos\left(\varphi_R - \varphi_O\right)$$

Thus H represents the illumination of the holographic material at the time of the exposure. The received energy W is a function of the exposure time Δt and the illumination time so that :

$$W = \int_{t_1}^{t_1+\Delta t} H \;\; dt = \Delta t\, |R|^2 + \Delta t\, |O|^2 + \Delta t\; R^* O + \Delta t\; R O^*$$

The principal physical factors which characterise a photosensitive plate are the transmission factor $|t|^2 = I_t / I_0$ where I_0 is the incident flux and I_t is the flux transmitted by the recording plate after its processing, the optical density of the negative, $DO = \log\left(1/|t|^2\right)$, the saturation of the plate $(\mathrm{W/cm^2})$ and the average sensitivity of the latter $(\mathrm{J/cm^2})$.

The characteristic curve which connects the amplitude transmission with the photosensitive plate gives a linear zone centred on the exposure W_0. The principal specificity of this plate is based on the following fact : if we take a sinusoidal exposure of the type $W = W_0 + \Delta W \cos(\varphi)$ in the recording linearity zone, then the amplitude transmission of the negative will be proportionate to the received illumination and we would get $t = t_0 - \beta \Delta W \cos(\varphi)$, as we can see in figure 3. The coefficient β represents the derivative of the transmittance against the exposure at the coordinates (W_0, t_0) for the average exposure.

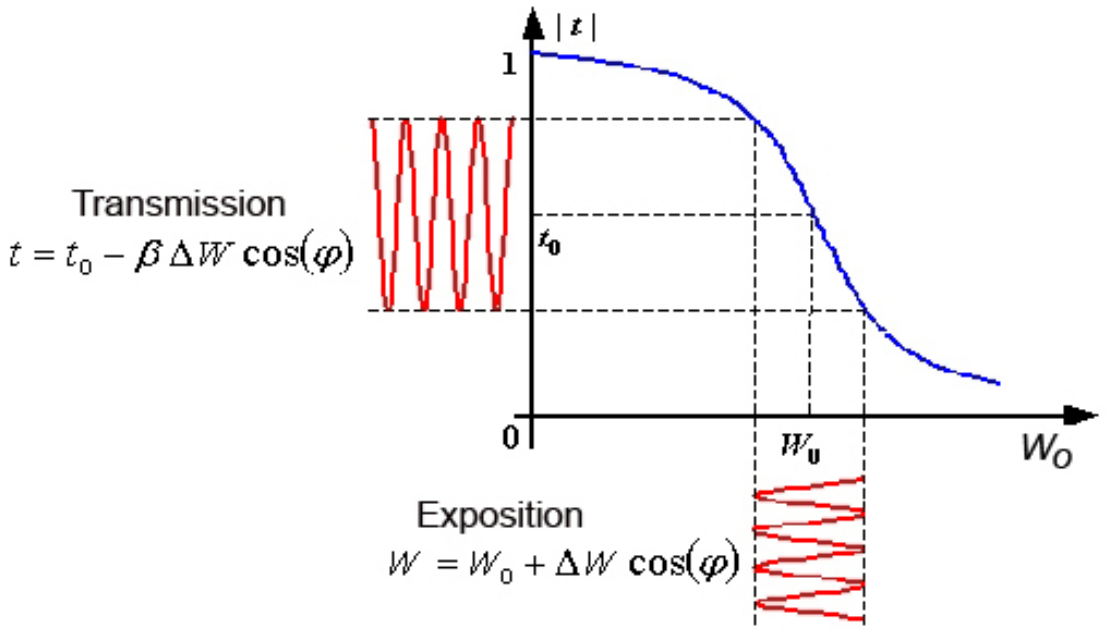

Figure 3 : Curve of the amplitude transmission against the exposure on a recording plate

Once the recording has been completed, the photosensitive plate is generally developed in a chemical bath in order to obtain a negative which encodes the phase and the amplitude of the wave from the studied object. In the linearity zone, the complex amplitude transmission t of the negative is combined with the energy received by the photosensitive plate as per the following equation :

$$t = t_0 - \beta (W - W_0)$$

The average amplitude transmittance for this average exposure is annotated t_0. The value of W shouldn't go too far away from the operating point in order to stay within the linear transmission zone, which means that the sinusoidal fringes needs to be slightly adjusted. W_0 represents the average value of the exposure and is written as :

$$W_0 = \Delta t |R|^2 + \Delta t |O|^2$$

Thus we get : $t = t_0 - \beta'(R^* O + R O^*)$ with $\beta' = \beta \Delta t$.

Remarque

These equations show that the phase and the amplitude of the object wave front are recorded (or encoded) on the holographic plate. It should be noted that the recording of the phase is important because it is the phase which gives the impression of depth during the reproduction of the object wave front by stereoscopy. After recording, each element on the surface of the holographic plate contains all the information of the initial object field seen from a given angle.

c) Transmission Holography

Transmission holography is the most widespread type. During the recording of the hologram the wave diffracted by the object and the reference wave are recombined on the same side of the photosensitive plate.

There are two possible recording configurations: the "**off axis**" configuration and the "**in line**" configuration.

The "in line" configuration was the first to be used by Gabor. The reference beam and the object beam come from the same direction, illuminating the same side of the photosensitive plate. The studied object is placed between the light source and the photosensitive plate. This configuration doesn't require a particularly coherent light source.

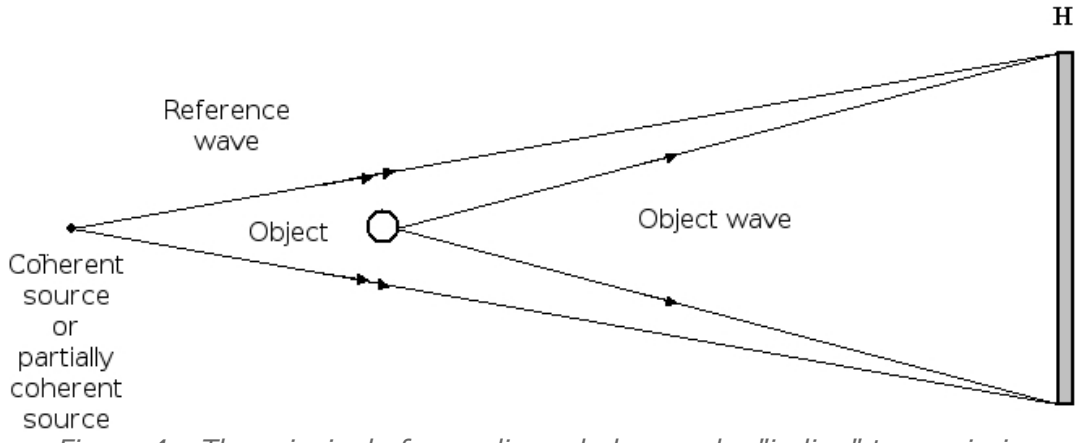

Figure 4 : The principal of recording a hologram by "in line" transmission

It has only been possible to use the "off axis" configuration since the invention of lasers because this configuration requires the use of a highly coherent light source. The object beam and the reference beam are mixed together. The off axis recording system is represented by figure 5.

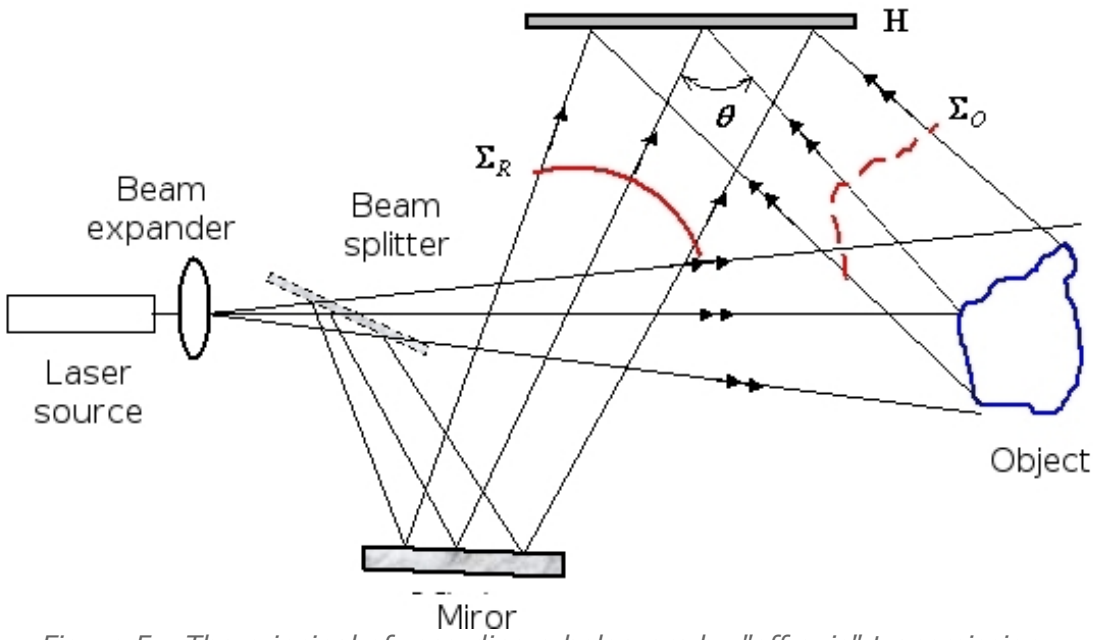

Figure 5 : The principal of recording a hologram by "off axis" transmission

The light source must, in this case, be highly spatially and temporally coherent apart from when a perfect equilibrium can be assured between the abject and reference optical paths. Lasers fit these requirements. **The coherence length is the determining parameter** : this characteristic defines the acceptable difference between optical paths so that there is interference between the two waves.

d) Reflection Holography

During the recording of the hologram, the two waves both illuminate a different side of the photosensitive plate. The reference wave and the object wave are propagated in opposite directions and cause interference on the interference plane (figure 6).

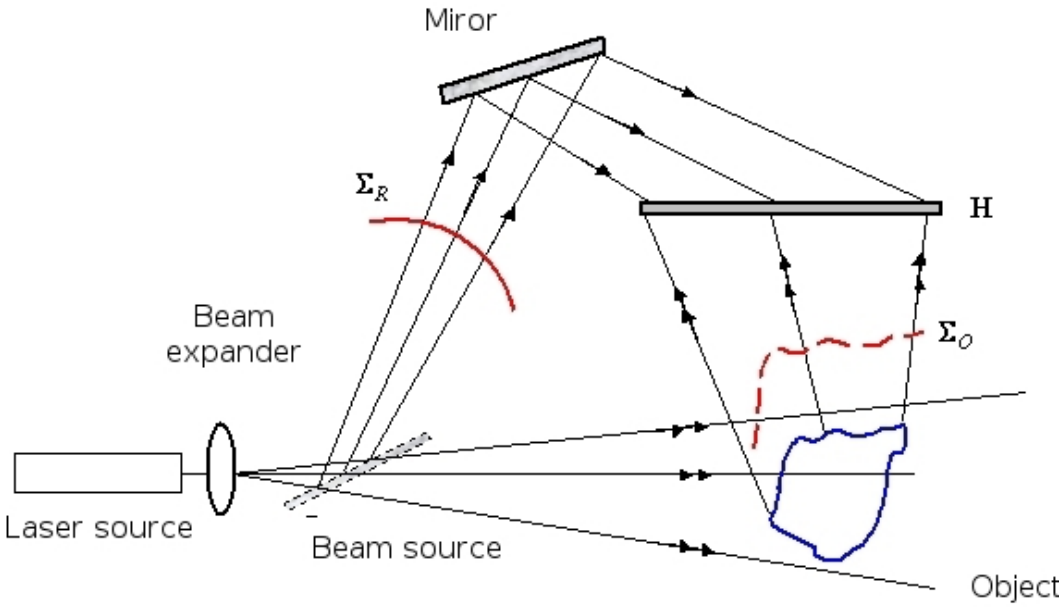

Figure 6 : The principal of recording a hologram by reflection : two-wave interferences

Another technique consists of using a single laser beam which serves as both the object beam and the reference beam (figure 7). This method was proposed by Y.Denisyuk [5 [Photographic Reconstruction of the Optical Properties of an Object in its Own Scattered Radiation Field]]. The reference beam directly illuminates the holographic plate and illuminates the object, which is situated behind the plate, at short range. The wave, thus diffracted by the object, interferes with the reference wave at the level of the photographic plate (with emulsion on the object side). This system has the advantages of using just one laser beam, which makes it easier to carry out. The object field can thus be viewed in white light.

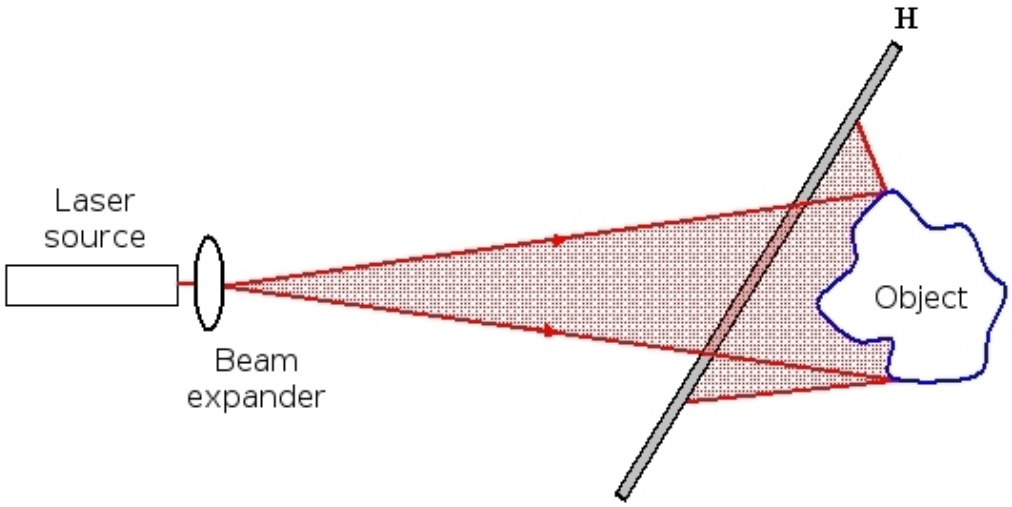

Figure 7 : Denisyuk's hologram

However, even though the quality of the reconstruction is realistic, the limited depth of the holographic field remains a major inconvenience. As with all reflection holograms, Denisyuk's holograms need to be "blanched", that is to say transformed in to a phase hologram, before being fixed, so that their image can have sufficient clarity and luminosity.

e) The different photosensitive plates

In order to obtain a reasonable recording of the hologram, it is necessary for the material to be sensitive to the wave length of the monochromatic light source which is used. The response to the illumination of the plate should show a good linearity. "Analogue" plates offer very good resolutions, generally higher than $1000\ \mathrm{mm}^{-1}$ ($<1\mu\ \mathrm{m}$)

Recorded holograms are divided into two categories :

- **Amplitude holograms** are made up of an interference pattern which results in a variation of either the transmission coefficient or the reflection coefficient in the recording plane; thus the amplitude of the reference beam is modulated by the hologram.
- **Phase holograms** encode the information using a variation in the refraction index or in the thickness of the photosensitive plate, which causes a modulation of the phase of the reference beam during reconstruction.

Table 1 sums up the principal materials which are used as photosensitive plates, the characteristics of these materials and the process of developing the negatives [6 [Holographie Industrielle],7 [Holographic Interferometry – Principles and Methods]].

Material	Processing	Hologram type	Exposition (J/m^2)	Spectral sensitivity (nm)	Resolution (mm^{-1})	Reusable
Silver halide	chimical	amplitude or phase	5×10^{-3}-5×10^{-1}	400-700	1000-10000	no
Bi-chromate gelatine	chimical	phase	10^{2}	350-580	>10000	no
Photo-resistant plane	chimical	phase	10^{2}	UV-500	3000	no
Photo-polymeres	post-exposition	phase	10-10^{4}	UV-650	200-1500	no
Photo-chromic plates		amplitude	10^{2}-10^{3}	300-700	>5000	yes
Photothermo-plastic plates	load and heating	phase	10^{-1}	400-650	500-1200	yes
Photorefractive $Bi_{12}SiO_{20}$		phase	**10**	350-550	10000	yes
Photorefractve $LiNbO_3$		phase	10^{4}	350-500	1500	yes

Tableau 1 : Characteristics of materails which are used as photosensitive plates

Silver halide photographic **emulsions** are the most used as recording materials; they have the advantage of being highly sensitive as well as presenting excellent spatial resolution. This type of plate allows the recording of both amplitude and phase holograms if a bleaching of the plate is carried out.

Bi-chromate gelatine allows for the production of phase holograms by photochemical reaction. The gelatine hardens depending on the level of illumination it is subjected to. The plate is simply washed with warm water in order to extract the gelatine which has not been exposed to the radiation. This material offers the best spatial resolutions.

Photo-resistant plates are organic photosensitive films. After the exposition and development stages, they produce phase holograms by variation of their thickness. They are rarely used because of their low sensitivity and because of the non-linear effects which are the product of low refractive efficiency.

Photopolymers are organic components which have the advantage of not needing to be treated by chemical solutions after exposure, thanks to photo-polymerisation. The information is encoded by variation of the thickness and the refraction index of the coating.

Photo-chromic plates have the considerable advantage of being reusable and don't require any preparation in the development stage. However, the given resolution is low compared to the silver photo plates. Because of their low sensitivity a high exposure time is required.

Photo-thermoplastic plates offer a certain ease of use given that they are reusable and can be developed on site, quickly and without chemical treatment. This type of plate used to be widely used in holographic interferometry [8 [A Quarter Century of Thermoplastic Holography]] it has almost fallen out of use nowadays, which has spurred on the development of digital holography.

Photorefractive crystals allow for the recording of a great number of phase holograms by photorefractive effect. They are often used in real-time in holographic interferometric applications [9 [Real Time Metrology With BSO Cristals]]. The spectral sensitivity of these crystals is relatively narrow. However, these solutions have been the object of commercialisation ; thus, the company Optrion [10] proposes a holographic camera which uses a BSO crystal as the recording plate. This camera is designed for photomechanical devices.

1.2. Reconstructing the object field

a) Principle of reconstruction by transmission

The reconstruction of the object field encoded within the hologram is based on **the principle of light diffraction**. If the holographic plate is illuminated after its development using the same reference wave used in the recording process, the light will diffract into three orders of diffraction if the diffraction network is sinusoidal. The complex amplitude which is transmitted is as follows :

$$\begin{aligned} A_R &= R\,t \\ &= R\,t_0 - \beta'|R|^2\,O - \beta'\,R^2\,O^* \end{aligned}$$

Respective to the three terms in this equation, the three orders of diffraction are : the 0-order, the $+1$-order and the -1-order.

- The -1-order is also called the real image; it is directly proportional to the conjugate complex of the object wave. This image is pseudoscopic, taking in to account its inverted contours (phase conjugation/retroflection) ;
- The 0-order is proportional to the sum of the squares of the modules of the two waves ;
- The $+1$-order is the most adapted to observation given that it is directly proportional to the original complex field. This order gives a virtual image and is characteristically orthoscopic.

During reconstruction using the "in line" configuration the three orders are superimposed and the virtual image is thus mixed with the real image and the direct transmission of the reference beam.

Figure 8 depicts the principle of reconstructing a hologram by "off axis" transmission. This configuration has the advantage of not causing the three orders to be superimposed during the reconstruction process, contrary to the "in line" configuration. The "off axis" system was used for the first time by Leith and Upatnieks [2 [Reconstructed Wavefront and Communication Theory],11 [Wavefront Reconstruction With Diffused Illumination and Three-Dimensional Objects]] following the invention of the first lasers.

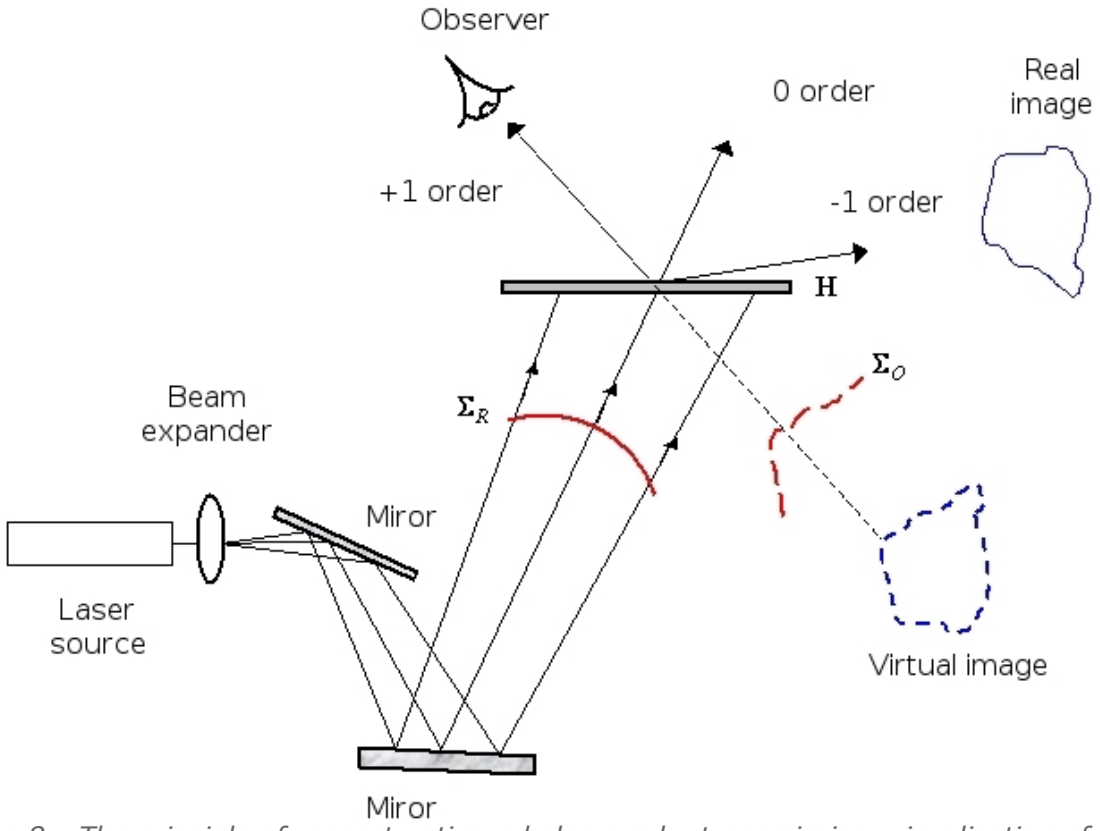

Figure 8 : The principle of reconstructing a hologram by transmission, visualisation of the virtual image

The way that a hologram is reconstructed makes it the reference wave which serves as the key for the decrypting of the encoded information. Indeed, the recording wave has a phase and amplitude distribution which is unique to that particular wave and this distribution is the key to the decoding.

It is possible to observe the real image by illuminating the plate with the complex conjugated component of the reference beam (figure 9).

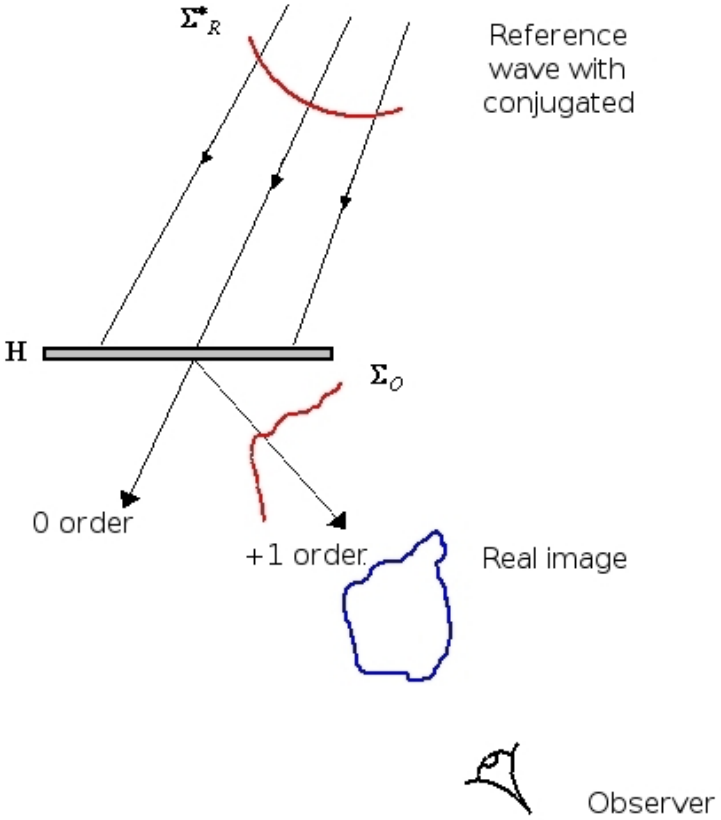

Figure 9 : The principle of reconstructing a hologram by transmission, visualisation of the real image

b) The principle of reconstruction by reflection

After the hologram has been recorded by the configuration shown in figure 6, the reconstruction is carried out according to the same principle which we have seen in transmission holography. Indeed, the hologram is illuminated by a beam which is identical to the reference beam, the latter is refracted by the holographic plate and the observer sees the image forming at the back of the plate. The image can be virtual or real.

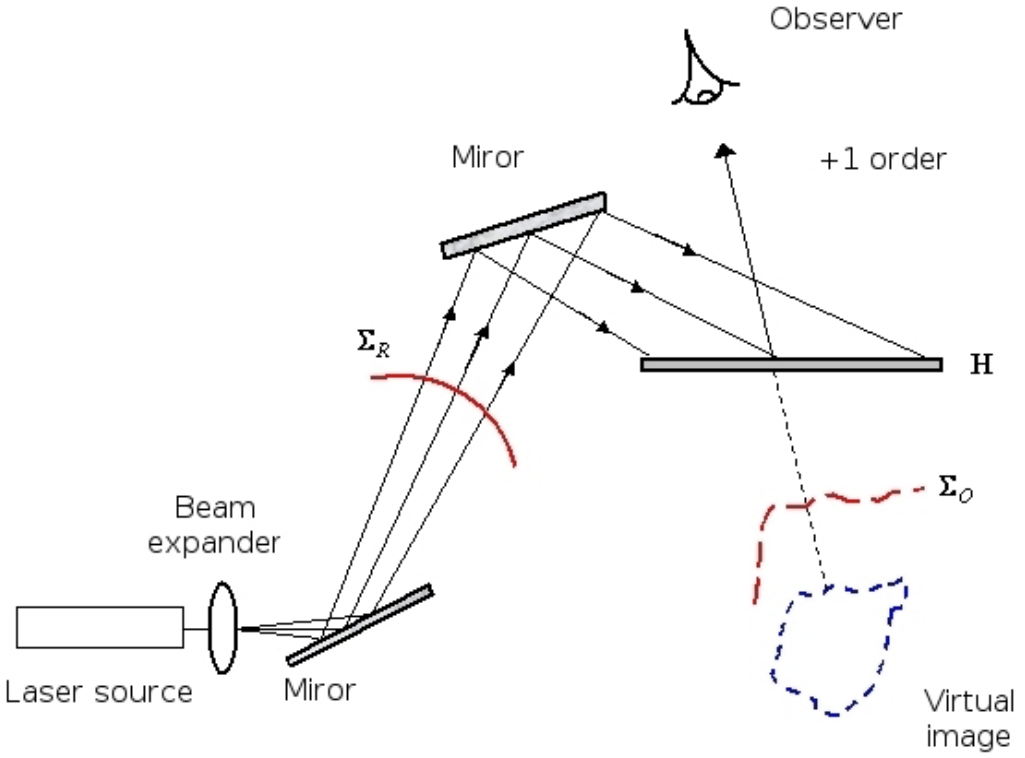

Figure 10 : The principle of reconstructing a hologram by reflection

c) Formation of the image in the +1-order

The formation of the image in this process of recording and reconstruction can be explained using **the diffraction formula**.

Let's consider that the observer is looking at the object reconstructed in the $+1$-order which conforms to the initial object. Let's also consider that the encoded hologram on the photosensitive plate is spatially limited by the physical size of the recording plate.

Note that Π_{L_x,L_y} is the function designating "the size of the photosensitive plate" :

$$\Pi_{L_x,L_y}(x',y')=\begin{pmatrix}1/L_x L_y & \text{if} \quad |x'|\le L_x/2 \quad \text{and} \quad |y'|\le L_y/2\\ 0 & \text{elsewhere}\end{pmatrix}$$

Where L_x and L_y are the width and the height of the plate.

The diffracted field in the $+1$-order, that is to say at the distance $-d_0$ from the plate, is expressed by Fresnel diffraction integral :

$$A_R^{+1}(x,y,-d_0)=\frac{j\beta' a_R^2}{\lambda d_0}\exp(-2j\pi d_0/\lambda)\exp\left(-\frac{j\pi}{\lambda d_0}(x^2+y^2)\right)$$
$$\times\int_{-\infty}^{+\infty}\int_{-\infty}^{+\infty}O(x',y',+d_0)\,\Pi_{L_x,L_y}(x',y')\exp\left(-\frac{j\pi}{\lambda d_0}(x'^2+y'^2)\right)\exp\left(+\frac{2j\pi}{\lambda d_0}(xx'+yy')\right)dx'\,dy'$$

Since the object field $O(x', y', d_0)$ can also be expressed by a Fresnel transform we get :

$$A_R^{+1}(x\,,\,y\,,-d_0)=-\frac{\beta'\,a_R^2}{\lambda^2\,d_0^2}\exp\left(-\frac{j\,\pi}{\lambda\,d_0}\left(x^2+y^2\right)\right)$$
$$\times\int_{-\infty}^{+\infty}\int_{-\infty}^{+\infty}\Pi_{L_x\,,\,L_y}(x'\,,\,y')\,F\left(\frac{x'}{\lambda\,d_0}\,,\,\frac{y'}{\lambda\,d_0}\right)\exp\left(+\frac{2\,j\,\pi}{\lambda\,d_0}\left(x\,x'+y\,y'\right)\right)dx'\,dy'$$

With

$$F\left(\frac{x'}{\lambda\,d_0}\,,\,\frac{y'}{\lambda\,d_0}\right)=\int_{-\infty}^{+\infty}\int_{-\infty}^{+\infty}\widetilde{F}(x\,,\,y)\exp\left(-\frac{2\,j\,\pi}{\lambda\,d_0}\left(x\,x'+y\,y'\right)\right)dxdy$$

And

$$\widetilde{F}(x\,,\,y)=A_0(x\,,\,y)\exp\left(j\,\psi_0(x\,,\,y)\right)\exp\left(+\frac{j\,\pi}{\lambda\,d_0}\left(x^2+y^2\right)\right)$$

Taking into account the properties of Fourier transforms, we finally get :

$$A_R^{+1}(x\,,\,y\,,-d_0)=-\beta\,\Delta t\,a_R^2\,A_0(x\,,\,y)\exp\left(j\,\psi_0(x\,,\,y)\right)*\widetilde{W}_A(x\,,\,y\,,-d_0)$$

With the enlargement function :

$$\widetilde{W}_A(x\,,\,y\,,-d_0)=\operatorname{sinc}\left(\frac{\pi\,L_x\,x}{\lambda\,d_0}\right)\operatorname{sinc}\left(\frac{\pi\,L_y\,y}{\lambda\,d_0}\right)$$

The reconstructed object in the $+1$-order is therefore proportional to the initial object field: it has the same amplitude and phase and thus the same contours and it is proportional to the exposure time and the transmittance gradient of the plate in the linear zone. Also, the reconstructed object is convoluted by an enlargement function $\widetilde{W}_A$ which is proportionnal to the size of the recording plate. The **convolution function** is a **two dimensional sinc function**. According to Rayleigh's criterion, this function has a width and height equal to :

$$R_x=\frac{\lambda\,d_0}{L_x}\ \text{ and }\ R_y=\frac{\lambda\,d_0}{L_y}$$

A nimerical application with the values $\lambda = 0.6328\mu\ \mathrm{m}$, $d_0 = 500\ \mathrm{mm}$ for a silver photo plate of $10 \times 12\ \mathrm{cm}^2$ gives $R_x = 2.63\mu\ \mathrm{m}$ and $R_y = 3.19\mu\ \mathrm{m}$.

These quantities determine the resolution in the image plane of the $+1$-order.

Remarque

The spatial resolution is thus proportional to the recording distance and inversely proportional to the width of the recording plate. In order to increase the resolution, the object must be placed nearer to the photo plate, using the largest possible photo plate.

2. Digital Holography

"Digital" holography differs from "analogue" holography (described above) in terms of the recording materials which are used and in the image reconstruction process for the studied object. The reconstruction of the phase and amplitude information of the object is carried out by the digital simulation of reference wave diffraction in the "digital hologram".

2.1. Digital Recording

Firstly, let's concern ourselves with the discretisation effect of the pixelated recording material. As we have already mentioned, digital holography dates form the 1970s and became more seriously accessible from the beginning of the 1990s.

The main advantage of digital photosensitive material is that the image is acquired quickly without having the chemical development stage, which represents a considerable time gain. Another advantage is that these plates are reusable once the data is stored.

The image sensor is now replacing the analogue photosensitive plate. The process for a recording a digital hologram is similar to that used in classic holography, in that the object diffracts a wave which interferes with the reference wave in the recording plane.

However, the spatial discretisation of the recorded pattern and the dimensions of the pixel elements impose certain conditions on the recording of a hologram. It is considered that the recording plate is a pixel matrix. The recording of a hologram on a digital photo plate not only discretises the photo plane but also integrates the temporal and spatial flux onto it. Whatever technology is used, the digital recording will (depending on the directions x' and y' on the recording plane) consist of, $N \times M$ pixels at a pitch of $p_x \times p_y$. Each of these pixels is of a dimension $\Delta_x \times \Delta_y$.

Figure 11 depicts the pixel matrix.

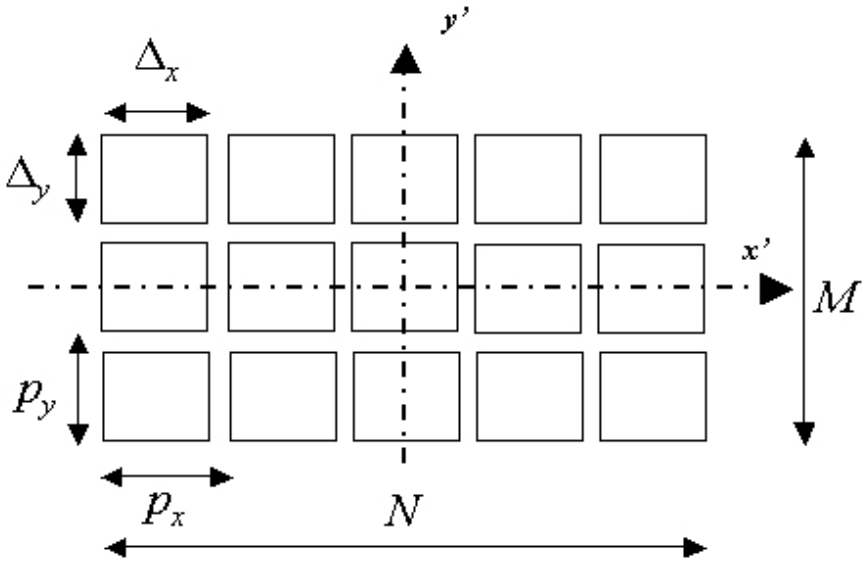

Figure 11 : Concept diagram of a surface-pixel sensor

As far as sensor technology is concerned, we mainly talk about CCD (charge-coupled device) sensors and CMOS (complementary metal-oxide-semiconductor) sensors. Matrices made up of photosensitive elements called pixels are generally square-shaped. Their size varies from $3\mu\,\mathrm{m}$ to $15\mu\,\mathrm{m}$. Thus, the spatial resolution of such sensors is between $66\,\mathrm{mm}^{-1}$ and $333\,\mathrm{mm}^{-1}$,

values which should be compared with those given in table 1 for so-called "analogue" recording materials.

Pixelised sensors offer by far the worst spatial resolution for the recording of holograms. The way these devices work is based on the photoelectric effect which causes the conversion of incident photons into electrons with a quantum efficiency of η_e. Silicon is the main element among the photosensitive elements. The sensor encodes the image using between 8 and 16 bits and each pixel contains N_e electrons at saturation point. The value of N_e is several tens of thousands of electrons, typically between $10,000$ and $40,000$. the average sensitivity of these sensors can be evaluated for comparison purposes with the values given in table 1.

As the pixels have a surface area of $\Delta_x \times \Delta_y$, the average necessary exposure needed to fill half the quantum well, is given by :

$$E_\lambda = \frac{h\, c\, N_e}{2\, \eta_e\, \lambda\, \Delta_x\, \Delta_y} \quad (\mathrm{J/m^2})$$

Where $h = 6.626176 \times 10^{-34}\mathrm{J.s}$ is the Planck constant and $c = 2.99792458 \times 10^{8}\ \mathrm{m.s^{-1}}$ is the speed of light in the vacuum.

A digital device with $\Delta_x = \Delta_y = 4.65 \times 10^{-6}\ \mathrm{m}$, $\eta_e = 0.4$, $N_\varepsilon = 30000$ and $\lambda = 0.5 \times 10^{-6}\ \mathrm{m}$ gives $E_\lambda = 6.8 \times 10^{-4}\mathrm{J/m^2}$. Silicon-based matrix sensors are therefore on average more than ten times more sensitive than the photosensitive plates listed in table 1.

Given the spatial extension of the pixels, the hologram at a certain coordinates $(x', y') = (k\, p_x, l\, p_y)$ can be written :

$$\begin{aligned} H_{PIX}(k\ p_x, l\ p_y, d_0) &= \int_{k\ p_x - \Delta_x/2}^{k\ p_x + \Delta_x/2} \int_{l\ p_y - \Delta_y/2}^{l\ p_y + \Delta_y/2} H(x', y', d_0)\, dx'\, dy' \\ &= \int_{-\infty}^{+\infty} \int_{-\infty}^{+\infty} H(x', y', d_0)\, \Pi_{\Delta_x, \Delta_y}(x' - k\ p_x, y' - l\ p_y)\, dx'\, dy' \end{aligned}$$

With the pixel function :

$$\Pi_{\Delta_x, \Delta_y}(x, y) = \begin{pmatrix} 1/\Delta_x \Delta_y & \text{if} \quad |x| \le \Delta_x/2 \quad \text{and} \quad |y| \le \Delta_y/2 \\ 0 & \text{elsewhere} \end{pmatrix}$$

The pixel function is even. The pattern of interferences recorded by a pixel at the coordinates $(k\, p_x, l\, p_y)$ is mathematically represented by a convolution product of the analogue hologram by the pixel function :

$$H_{PIX}(k\ p_x, l\ p_y, d_0) = \left[H(x', y', d_0) * \Pi_{\Delta_x, \Delta_y}(x', y') \right](k\ p_x, l\ p_y)$$

The digital hologram recorded as an image is a juxtaposition, depending on the two dimensions, of all the integration surfaces. This image is mathematically represented by the following relationship :

$$H_N(x', y', d_0) = \sum_{k=0}^{k=N-1} \sum_{l=0}^{l=M-1} H_{PIX}(k\ p_x, l\ p_y, d_0)\, \delta(x' - k\ p_x, y' - l\ p_y)$$

The pixel function therefore has a smoothing effect which is to say of by low pass filtering over the raw hologram.

Remarque

Thus, the recording of a digital hologram can be classified as a "low resolution" recording while recording using the "analogue" silver photo plates are classed as "high resolution".

2.2. Constraints on digital recording

As has already been mentioned at the beginning of this course, a hologram is a speckle pattern (laser granularity) which corresponds to the interaction between a reference wave and a diffracted object wave, the latter also of "speckle" composition. In terms of zones, the interference fringes generated by two monochromatic plane wave, at an angle of θ, apart, have an inter-fringe distance (figure 12) of :

$$i = \frac{\lambda}{2 \sin\left(\frac{\theta}{2}\right)}$$

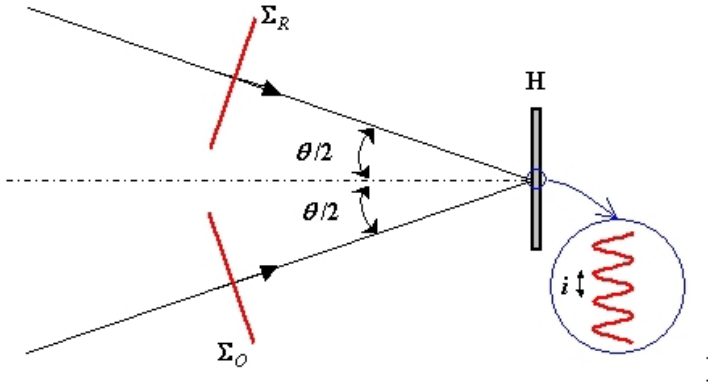

Figure 12 : Local fringes

The angle θ imposes almost no constraints in classical holography given the high resolution capability of analogue recording plates. The pixel pitch of current sensors, in digitally acquiring images, is limited. However, their resolution must be sufficiently high in order that the inter-fringe distance corresponds to at least 2 pixels.

The **Shannon theorem** indicretes that for the correct acquisition of a given periodic signal, the sample frequency must be at least twice as high as the signal frequency. Otherwise, there would be a loss of information due to the weak sampling level. Thus, the first recording condition to be respected is that imposed by the Shannon criteria :

$$f_e \geq 2\, f_s$$

where f_e is the sampling frequency and f_s is the signal frequency which are being studied. Let's consider the case of a digital recording sinusoidal fringes; the sampling frequency f_e corresponds to the inverse of the pitch between two consecutive pixels within the sensor (p_x or p_y depending on the studied dimension), and the studied signal frequency is the reciprocal of the inter-fringe distance i. That is to say :

$$f_e = \frac{1}{\max\left(p_x\,,\, p_y\right)}$$

And

$$f_s = \frac{1}{i} = \frac{2\sin(\theta/2)}{\lambda}$$

Since the size of the pixels is fixed, the spatial sampling cannot be increased. In order to create good recording conditions, the angle between the object and the reference beams must be adapted.

Remarque

Thus, taking into account the three previous equations, the Shannon criteria results in the following disparity :

$$\theta_{max} \leq 2\sin^{-1}\left(\frac{\lambda}{4\max(p_x, p_y)}\right)$$

For a wave length of $633\ \text{nm}$ and a pitch between the pixels of $4.65\mu\ \text{m}$, the maximum angle, corresponding to the limits of the Shannon criteria, is $\theta_{max} = 3.9$. The small angular deviation which is thus permitted between the two beams requires the use of a relatively precise adjustment device.

2.3. Different recording configurations

a) Introduction

It is possible to record a hologram using various different configurations which sometimes move away from the basic principle of holography whilst keeping a strong correlation with holography as far as recording the interferometric pattern is concerned. A convergent or divergent lens between the object and the matrix sensor is often used. Generally, it is preferred that the reference wave is plane $(r_0 = \infty)$, so that its phase is simply written :

$$\varphi_R(x', y') = 2\pi\left(u_R x' + v_R y'\right)$$

b) Fresnel's digital holography

Diffraction using the Fresnel approximation requires that the finite distance between the object and the recording plane be taken into account. Figure 13 represents the recording device. The reference wave is plane and can follow the object wave axis for "in line" configuration recording or it can set up an angle with the object wave for "off axis" configuration recording. The device is the most widespread for the digital recording of interference patterns [12 [Methods of Digital Holography : a Comparison]].

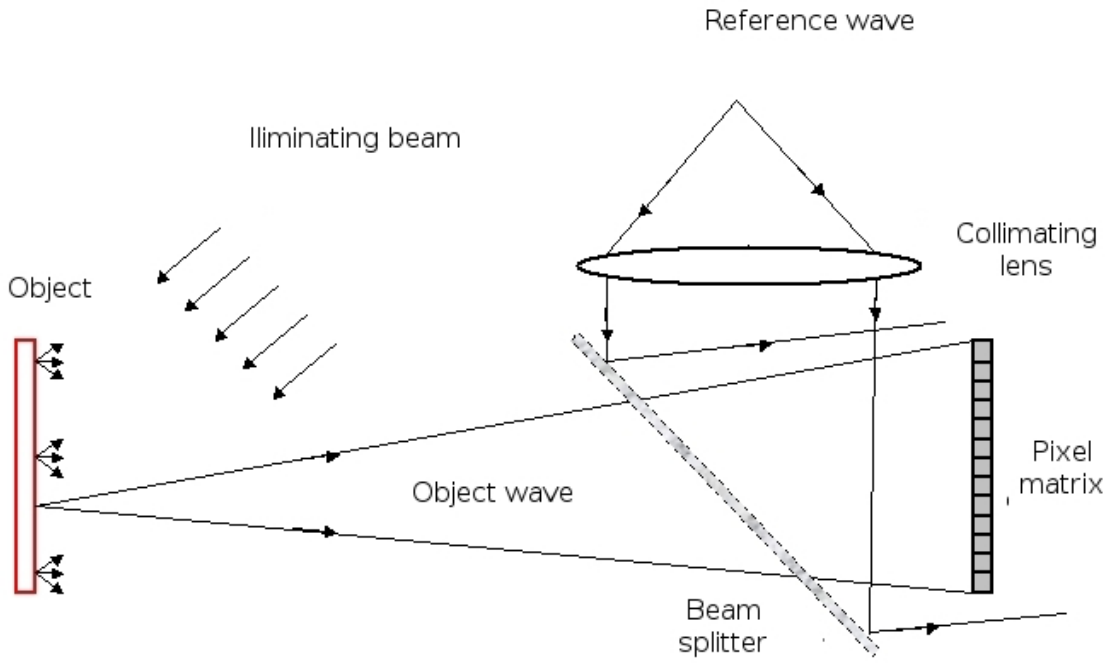

Figure 13 : Frenel's digital recording device

The distance between the object and the pixel matrix must follow the Fresnel conditions [13 [Introduction to Fourier Optics]].

c) Fraunhofer's digital holography

The recording device, depicted in figure 14, sees the object placed in the focal plane of a convergent lens.

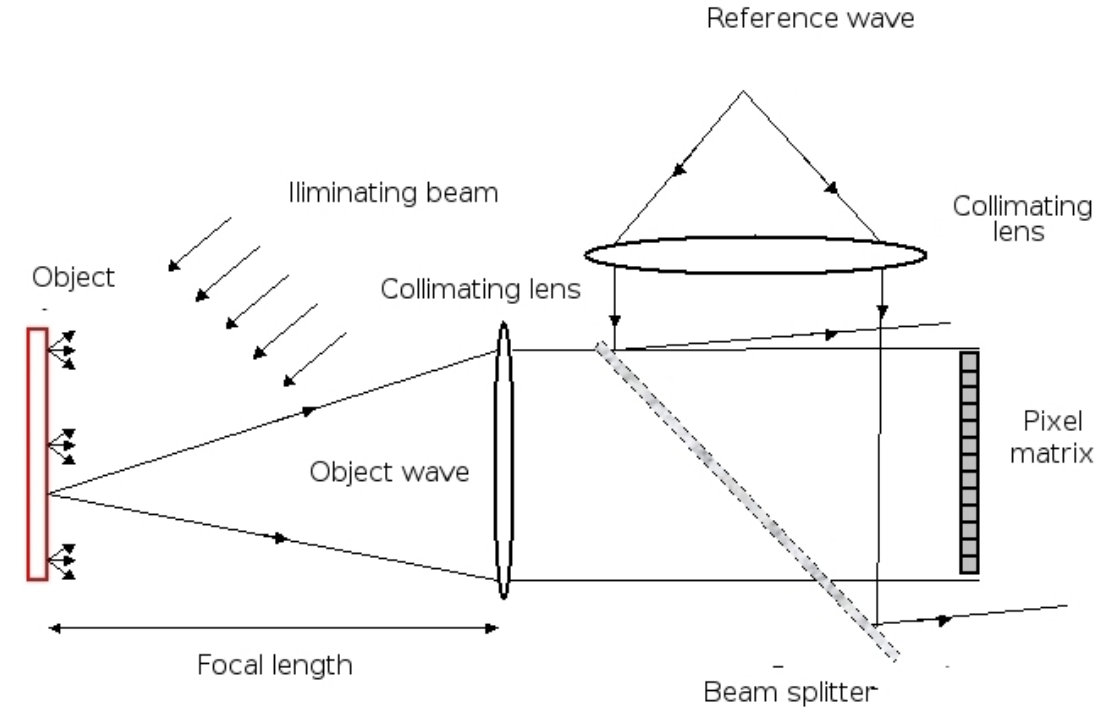

Figure 14 : Fraunhofer's digital recording device

The role of the lens is to collimate the beam diffracted by the object. This configuration allows one to balance out the quadratic phase term by adjusting the transmittance pattern in the Fresnel diffraction integral. Thus, the effective distance between the object and the recording plane is infinite relative to the object and sensor apertures.

This configuration corresponds with the **Fraunhofer conditions**. Generally, the hologram is categorized as a **Fourier hologram** since a simple Fourier transform is sufficient to reconstruct the object field .

2.4. Methods for reconstructing the object wave front

a) Introduction

Two methods are presented in this chapter :

- The reconstruction of the complex object field by the Fresnel transform ;
- And the convolution reconstruction method.

Both are based on the Fresnel-Kirchhoff diffraction integral.

b) Reconstruction using a discrete Fresnel transform

Let's consider that instead of a classic diffracting aperture that we have a discrete transmittance; this represents a hologram recorded beforehand on a pixel matrix. We have already seen that the object wave is reconstructed by diffracting the reference beam onto the holographic plate. In order to obtain phase and amplitude information from the initial field, the diffraction of the incident reference wave must be simulated on the transmittance matrix.

The Fresnel diffraction integral is discretised by replacing the double integral with a double summation and the recording plane coordinates are sampled with a pitch which corresponds to that of the pixel matrix, that is to say $(x', y') = (k\,p_x, l\,p_y)$, where k and l vary from 0 to $N-1$ and from 0 to $M-1$.

Also, since the processor cannot calculate an infinite number of points in the reconstructed field, the discreet nature of the image plane must also be taken into account. In particular, it is necessary to consider the nature of the Fresnel integral: it is a two-dimensional Fourier transform. The classic rules for time and frequency sampling which are applied to the digital processing of the classic signal are also essential in this case. For the recording of a digital hologram at a reconstruction distance d_R , the discret eFresnel transform is written :

$$A_R(X, Y, d_R) = -\frac{j}{\lambda\, d_R}\exp\left(+2\,j\,\pi\, d_R/\lambda\right)\exp\left(+\frac{j\,\pi}{\lambda\, d_R}\left(X^2+Y^2\right)\right)$$
$$\times \sum_{k=0}^{k=N-1}\sum_{l=0}^{l=M-1} H_{PIX}(k, l, d_0)\exp\left(+\frac{j\,\pi}{\lambda\, d_R}\left(k^2\,p_x^2+l^2\,p_y^2\right)\right)\exp\left(-\frac{2\,j\,\pi}{\lambda\, d_R}\left(X\,k\,p_x+Y\,l\,p_y\right)\right)$$

At this point, it must be noted that in this calculation it is not obligatory to take the reference beam into account if it is plane and uniform $(a_R(x', y') = C^{te})$, contrary to the case of physical reconstruction using a laser which requires illumination with a reference beam. In the case of a spherical wave $(r_0 \neq \infty)$, it would be necessary to take the curvature of the wave front into account and to multiply H_{PIX} by an appropriate complex term.

c) The discretisation of the reconstructed plane

According to the expression for the discrete Fresnel transform, the apparent sampling periods of the exponential function, which gives the Fourier character of the integral, are shown by :

$$T_{ex} = \frac{p_x}{\lambda\, d_R} \qquad T_{ey} = \frac{p_y}{\lambda\, d_R}$$

If the reconstructed field is calculated using the same number of points $(M \times N)$ that is pixels in the detector, the sampling pitch in the image plane is equal to :

$$\Delta\,\eta = \frac{1}{N\; T_{ex}} = \frac{\lambda\, d_R}{N\;\; p_x} \qquad \Delta\,\xi = \frac{1}{M\; T_{ey}} = \frac{\lambda\, d_R}{M\;\; p_y}$$

Consequently, the sampling in the image plane is simply :

$$X = n\,\Delta\,\xi \qquad Y = m\,\Delta\,\eta$$

where n and m vary from $-N/2$ to $N/2 - 1$ and from $-M/2$ to $M/2 - 1$.

Zero-padding (extending the pixel matrix with zeros) will be discussed later on. The discrete version of the Fresnel integral is ultimately written :

$$A_R(n\,,\,m\,,\,d_R) = \frac{-\,j}{\lambda\, d_R}\exp\left(+2\;j\;\pi\;d_R/\lambda\right)\exp\left(+\frac{j\;\pi}{\lambda\;d_R}\left(n^2\;\Delta\;\xi^2 + m^2\;\Delta\;\eta^2\right)\right)$$
$$\times \sum_{k=0}^{k=N-1}\;\sum_{l=0}^{l=M-1} H_{PIX}\left(k\;,\,l\;,\,d_0\right)\exp\left(+\frac{j\;\pi}{\lambda\;d_R}\left(k^2\;p_x^2 + l^2\;p_y^2\right)\right)\exp\left(-\,2\;j\;\pi\left(\frac{n\,k}{N} + \frac{m\,l}{M}\right)\right)$$

This relationship expresses the reconstructed field at the pixel coordinates (n, m) in the image plane. With only one phase factor, the reconstructed field is proportionate to a discrete two-dimensional Fourier transform (FFT = Fast Fourier Transform) of the product of the digital hologram multiplied by a discrete quadratic phase term.

The algorithm for reconstruction using the discrete Fresnel transform is shown in figure 15.

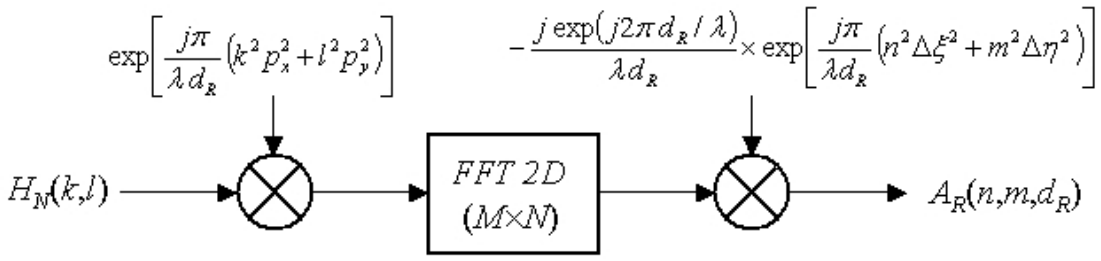

Figure 15 : Algoritm for the Fresnel transform

If one were to choose $d_R = -d_0$, then the $+1$-order would be in focus in the reconstructed field. If, on the other hand, one were to choose $d_R = +d_0$, it would be the -1-order that was in focus.

d) Constraints on the reconstruction distance

The reader should note that the application of this algorithm requires a discrete version of the quadratic phase term of the Fresnel transform to be programmed. The sampling of this complex oscillating function is necessary in order to respect the Shannon conditions.

In order to do this, one only needs to consider the spacial frequency content of the function in terms of spatial frequencies [15 [Digital Holography for Quantitative Phase Contrast Imaging]]. Let's consider the phase of the quadratic term :

$$\exp\left(\frac{j\,\pi}{\lambda\,d_R}\left(x^2+y^2\right)\right)=\exp\left(j\,\Theta\left(x\,,\,y\right)\right)$$

The spatial frequencies are given by :

$$u_i=\frac{1}{2\,\pi}\,\frac{\partial\,\Theta\left(x\,,\,y\right)}{\partial\,x}\qquad\qquad v_i=\frac{1}{2\,\pi}\,\frac{\partial\,\Theta\left(x\,,\,y\right)}{\partial\,y}$$

Giving

$$u_i=\frac{1}{2\,\pi}\,\frac{\partial}{\partial\,x}\,\frac{\pi\,x^2+\pi\,y^2}{\lambda\,d_R}=\frac{x}{\lambda\,d_R}\qquad\qquad v_i=\frac{1}{2\,\pi}\,\frac{\partial}{\partial\,y}\,\frac{\pi\,x^2+\pi\,y^2}{\lambda\,d_R}=\frac{y}{\lambda\,d_R}$$

The quadratic term is a signal with an unstationary character since its frequencies $\{u_i, v_i\}$ vary according to the evolution variables $\{x, y\}$. In theory, the energy of the signal is infinite.

However, the signal must be considered within the confines of a limited space – that of the sensor's pixel space. Delimiting its evolution horizon imposes a limit on its energy and on its frequential content. The size of x and y is restricted by $[-x_{max}, +x_{max}]$ and $[-y_{max}, +y_{max}]$ which correspond to the recording scale ($N \times M$ pixels at a pitch of $p_x \times p_y$, sensor $N\,p_x \times M\,p_y$), this is to say $x_{max} = N\,p_x/2$ and $y_{max} = M\,p_y/2$.

Thus, the maximum spatial frequencies of the signal are given by :

$$u_i^{max}=\frac{x_{max}}{\lambda\,d_R}\qquad\qquad v_i^{max}=\frac{y_{max}}{\lambda\,d_R}$$

Within the sensor, the bilateral spatial bandwidth of the quadratic term is therefore :

$$\Delta\,u=2\,u_i^{max}=\frac{N\,p_x}{\lambda\,d_R}\qquad\qquad \Delta\,v=2\,v_i^{max}=\frac{M\,p_y}{\lambda\,d_R}$$

Thus, the bandwidth reduces when the distance increases. The Shannon theory imposes the following :

$$f_{ex}\geq 2\,u_i^{\max}=\Delta\,u=\frac{N\,p_x}{\lambda\,d_R}\quad\text{ and }\quad f_{ey}\geq\Delta\,v$$

Since the pixel pitch is imposed by the technology being used, the minimum distance d_R which represents the Shanon criteria is given by :

$$d_R\geq\sup\left\{\frac{N\,p_x^2}{\lambda}\,,\,\frac{M\,p_y^2}{\lambda}\right\}$$

Table 2 sums up the minimum distances according to the acquisition parameters.

Matrix	Pixel (μ m)	Warelength	Minimum distance
512×512	01/04/65	632.8	17/05/09
1024×1024	01/04/65	632.8	35
2048×2048	01/04/65	632.8	70

Tableau 2 : Minimum reconstruction distances

This result imposes a minimum distance for reconstruction using the Fresnel transform.

e) Expression of the digital +1-order

The analytical calculation of the diffracted field in the $+1$-order must take into account the active pixel surface, the comparative lack of focalization in digital holography and the possible surface aberration of the reference beam. This calculation will not be analysed in this course. Instead, we have settled for outlining the principal result in the case of the pixel being infinitely localised $(\Delta x = \Delta y = 0)$ and for $d_R = -d_0$ where we have $(X, Y) = (x, y)$.

From the equation of the discreet Fresnel transform, we get that the digitally diffracted field in the $+1$-order is shown by :

$$A_R^{+1}(x, y, -d_0) = \lambda^2 d_0^2 \exp\left(-j \pi \lambda d_0 \left(u_R^2 + v_R^2\right)\right) R^*(x, y) \; A(x, y) * \tilde{W}_{NM}(x, y, -d_0) * \delta(x - \lambda d_0 u_R, y - \lambda d_0 v_R)$$

With

$$\tilde{W}_{NM}(x, y, -d_0) = \exp\left(-j \pi (N-1) \frac{x\, p_x}{\lambda \% d_0} - j \pi (M-1) \frac{y\, p_y}{\lambda d_0}\right) \times \frac{\sin(\pi N x p_x / \lambda d_0)}{\sin(\pi x p_x / \lambda d_0)} \frac{\sin(\pi M y p_y / \lambda d_0)}{\sin(\pi y p_y / \lambda d_0)}$$

And $\delta(x, y)$ is the two-dimensional Dirac distribution. The $+1$-order is therefore located at the coordinates $(\lambda d_0 u_R, \lambda d_0 v_R)$ in the reconstructed plane. These coordinates depend on the spatial frequency of the reference wave and the reconstruction distance.

As we saw in paragraph A.2.c, the reconstructed object is also convoluted by an enlargement function $\tilde{W}_{NM}$ which is linked to the size of the sensor. This function is the filter function of the two-dimensional discrete Fourier transform. Its mathematical form seems very different from that of the function $\tilde{W}_A$, however, its profile is similar to a two-dimensional sinc function.

This function imposes the pre-defined resolution on Fresnel digital holography. The interpretation of this function is quite simple : $\tilde{W}_{NM}$ is a digital diffraction puttern of a rectangular aperture of dimensions $N p_x \times M p_y$ with uniform transmittance. The resolution function is graphically represented in modulus in figure 16 for the following digital values : $N = M = 1024$, $p_x = p_y = 4.65\mu$ m, $\lambda = 0.6328\mu$ m and $d_0 = 500$ mm.

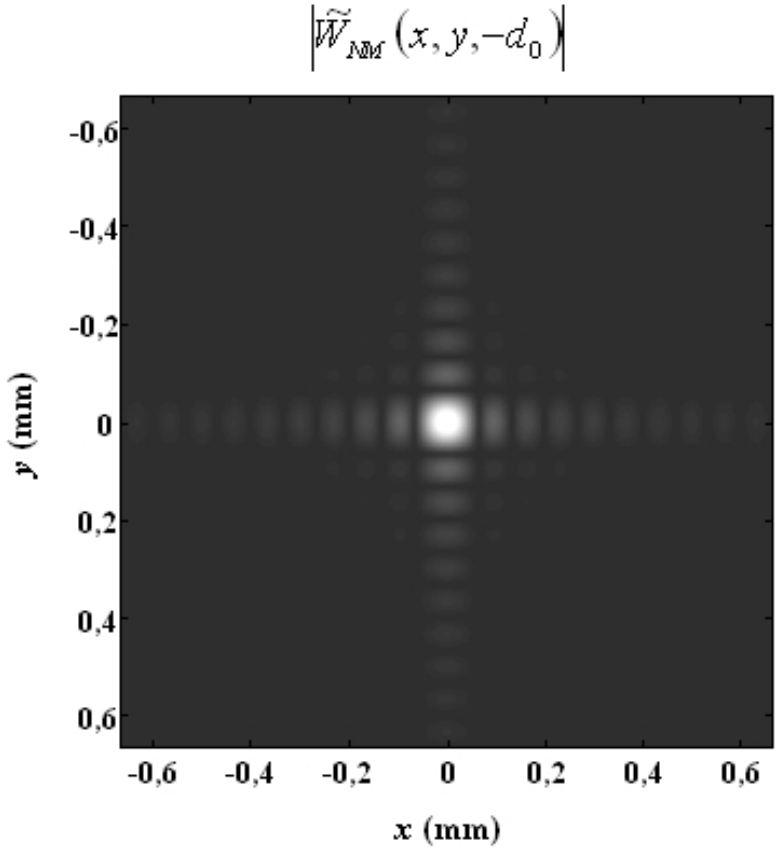

Figure 16 : Impulse response of the discrete Fresnel transform

According to the Raleigh criteria, this function has widths equal to :

$$R_x = \frac{\lambda d_0}{N p_x} \quad \text{and} \quad R_y = \frac{\lambda d_0}{M p_y}$$

These quantities set the resolution in the image plane. The spatial resolution is therefore proportional to the recording distance and inversely proportional to the width of the sensor.

A digital application with the values given above produces $R_x = R_y = 66.99\mu\,\mathrm{m}$. In comparison with digital applications with a silver plate of $10 \times 12\,\mathrm{cm}^2$, the spatial resolution is 21 to 25 times smoller.

f) Getting rid of the interference orders

The algorithm shown in figure 15 can be directly applied to the recorded hologram. In this case, the reconstructed field will systematically contain the three diffraction orders. In 1997 [21 [Phase Shifting Digital Holography]], Yamaguchi proposed applying the technique of fringe demodulation by phase shift to digital holography. The idea is that since the hologram is an interferometric composition of two waves, it is possible to extract the desired order by applying a phase shift to the reference wave.

Note that ϕ is the phase shift applied to the reference wave which is now written :

$$R(x', y') = a_R(x', y') \exp\left(j\,\varphi_R(x', y') + j\,\phi\right)$$

Let's choose 4 phase shift values :

$$\phi = \{0\ ,\ \pi/2\ ,\ \pi\ ,3\ \pi/2\}$$

Then, since H can also be written

$$H = a_R^2 + a_O^2 + 2\ a_R\ a_O \cos\left(\varphi_R - \varphi_O + \phi\right)$$

We can extract from each of the four recorded holograms, the phase of the diffracted object field φo and its amplitude a_O and we can also calculate the $+1$-order which corresponds with the term $O = a_O \exp\left(j\varphi_O\right)$. In fact at each point where the hologram is recorded :

$$a_O = \frac{1}{4\ a_R} \times \sqrt{\left(H\left(0\right) - H\left(\pi\right)\right)^2 + \left(H\left(3\ \pi/2\right) - H\left(\pi/2\right)\right)^2}$$

And

$$\varphi_O = \arctan\left(\frac{H\left(3\ \pi/2\right) - H\left(\pi/2\right)}{H\left(0\right) - H\left(\pi\right)}\right)$$

Then, applying the algorithm we have seen in figure 15 to the -1-order is all that is needed to form the image of the initial object on its own. This method is efficient as far as getting rid of the $+1$-order is concerned but it is over-the-top in recording terms since four holograms are re1quired to reform the object.

g) Zero-padding

It should be remarked that the sampling pitch of the image space depends on the number of points used in the reconstruction, on the wavelength, on the pixel pitch and on the reconstruction distance. There is therefore no invariance in the sampling pitch at the moment of reconstruction by the direct Fresnel transform.

As has been mentioned in one of the previous paragraphs, the diffracted field is estimated over a finite number of points. The calculation of the discreet Fresnel transform of the hologram can be carried out over points $L \times K$ as $(L, K) \geq (M, N)$.

- If $(L, K) = (M, N)$ then the raw interferogram is used in the digital calculation of the Fresnel transform.
- If $(L, K) > (M, N)$ one finds oneself in the situation of zero-padding (which basically means adding $(L - M, K - N)$ zeros to the pixel matrix).

Remarque

Fundamentally, these additional zeros do not add any rational information but they do modify the sampling pitch of the diffracted field.

Indeed, the pitch would now be given as :

$$\Delta\ \eta = \frac{\lambda\ d_R}{K\ p_x} \qquad \Delta\ \xi = \frac{\lambda\ d_R}{L\ p_y}$$

The sampling in the image plane is henceforth :

$$X = n\ \Delta\ \xi \qquad Y = m\ \Delta\ \eta$$

Where n and m vary from $-K/2$ to $K/2-1$ and from $-L/2$ to $L/2-1$.

We therefore know that $\Delta\eta < R_x$ and $\Delta\xi < R_y$. There is a reduction in the sampling pitch and thus an increase in the "definition" of the image plane.

In concrete terms, this means that we see a greater texture in the image : the zero-padding of the hologram has the consequence of making the speckle grain structure of the image appear more precise.

Remarque

However, zero-padding does not change the intrinsic resolution which is imposed by the number of pixels in the image sensor and the size of these pixels.

h) Reconstruction by convolution

Let's look again at the Fresnel-Kirchhofff diffraction integral expressed in Cartesian coordinates[[Introduction to Fourier Optics]] :

$$O(x',y',d_0)=\frac{d_0}{j\lambda}\int_{-\infty}^{+\infty}\int_{-\infty}^{+\infty}A(x,y)\frac{\exp\left(+2j\pi/\lambda\sqrt{d_0^2+(x'-x)^2+(y'-y)^2}\right)}{d_0^2+(x'-x)^2+(y'-y)^2}dx\,dy$$

This integral is also a convolution equation :

$$O(x,y,d_0)=A(x,y)*h(x,y,d_0)$$

With $h(x,y,d_0)$, the impulse response of the free space propagation, expressed by :

$$h(x,y,d_0)=\frac{d_0}{j\lambda}\frac{\exp\left(+2j\pi/\lambda\sqrt{d_0^2+x^2+y^2}\right)}{d_0^2+x^2+y^2}$$

In the framework of the Fresnel approximations, the impulse response becomes :

$$h(x,y,d_0)=\frac{1}{j\lambda d_0}\exp\left(\frac{2j\pi d_0}{\lambda}\right)\exp\left(+\frac{j\pi}{\lambda d_0}(x^2+y^2)\right)$$

And the diffracted field is expressed by the Fresnel transform which we have already seen at the beginning of this course :

$$O(x',y',d_0)=-\frac{j}{\lambda d_0}\exp(+2j\pi d_0/\lambda)\exp\left(+\frac{j\pi}{\lambda d_0}(x'^2+y'^2)\right)$$
$$\times\int_{-\infty}^{+\infty}\int_{-\infty}^{+\infty}A(x,y)\exp\left(+\frac{j\pi}{\lambda d_0}(x^2+y^2)\right)\exp\left(-\frac{2j\pi}{\lambda d_0}(xx'+yy')\right)dxdy$$

The impulsional response has a transfer function $\tilde{H}(u,v,d_R)$ so that :

$$\tilde{H}(u,v,d_R)=\int_{-\infty}^{+\infty}\int_{-\infty}^{+\infty}h(x,y,d_R)\exp(-2j\pi(ux+vy))dxdy$$

Applied to the reconstruction of the object field at the distance d_R, from the hologram H_N, the discreet version of the convolution equation is simply :

$$A_R(n, m, d_R) = \sum_{k=0}^{N-1} \sum_{l=0}^{M-1} H_{PIX}(k, l)\, h(k-n, l-m, d_R)$$

There are several ways to look at the practical use of this relationship. The simplest is to use the properties of the Fourier transform: the convolution of two functions can be processed by the inverse Fourier transform of the product of the Fourier transforms of each of the functions.

This property is used in digital holography, given that calculation by discrete Fourier transforms is less time consuming in terms of calculation than the convolution method (double summation as opposed to optimised algorithms).

Thus the reconstructed field at the distance d_R is calculated by application of the following equation :

$$A_R(k, l, d_R) = FFT^{-1}\left[FFT\left[H(k, l)\right](p, q) \times FFT\left[h(k, l, d_R)(p, q)\right]\right](k, l)$$

The algorithm for reconstruction by discrete convolution is given in figure 17.

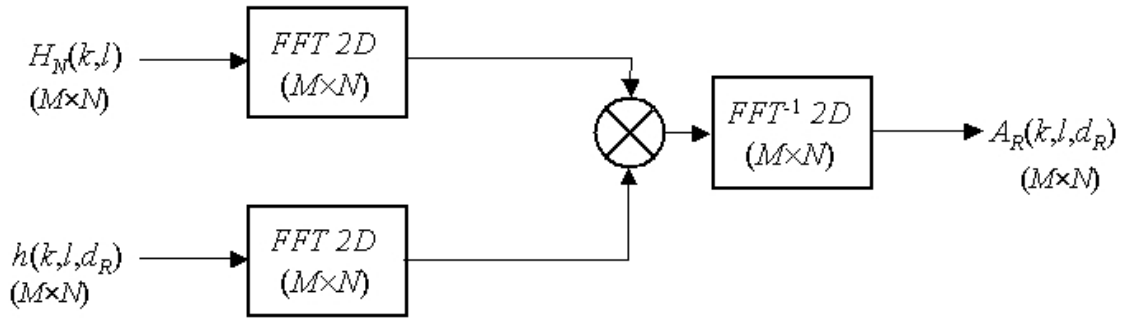

Figure 17 : Algorithm for reconstruction by discrete convolution

It is possible to apply this algorithm to just the $+1$-order, extracted from the hologram by the phase shift technique.

The reader should note that the reconstruction conditions which were outlined in the previous paragraph and which concern the minimum recording distance d_R are also valid in this case. If the exact impulse response [13 [Introduction to Fourier Optics]] is used we get :

$$d_R \geq \sup\left\{ \frac{N\ p_x \sqrt{4\ N^2\ p_x^2 - 1}}{\lambda}\ ,\ \frac{M\ p_y \sqrt{4\ M^2\ p_y^2 - 1}}{\lambda} \right\}$$

Let's consider the algorithm from figure 17: two Fourier transforms are used; a direct transform and then a reciprocal one. Because of this, the observation horizon of the reconstructed field is identical to that of the recorded hologram. This means that the sampling pitch in the image plane is identical to the pixel pitch, that is to say $\Delta\xi = p_x$ and $\Delta\eta = p_y$ contrary to the case of direct calculation where the pitch depends on the reconstruction distance.

Remarque

This method is thus recommended when the sampling pitch needs to stay constant in the different reconstructed planes.

i) Spectral scanning by the filter bank method

With the FFT digital convolution method, the maximum observation horizon is imposed by the size of the sensor matrix. If the object is larger than the pixel matrix, it is necessary to carry out a spectral scan in order to reconstruct the object by assembling adjacent pieces. In terms of spatial bandwidth, this means that the bandwidth of the impulse response is not sufficient to cover the spatial bandwidth occupied by the object. In this case, in order to put into place a reconstruction by convolution it is necessary to programme the filter bank so that its role is to carry out the spectral scanning which is necessary for the reconstruction of the whole object.

The number of required scans depends on the bandwidth of the filter. The relationship *between metric space and spatial frequency* shows that a holographic spatial frequency equal to (u_0, v_0) matches a point in the reconstructed object equal to $(\lambda d_R u_0, \lambda d_R v_0)$. The bandwidth of the impulse response allows an area, equal to $\Delta x = N\ p_x$ in width and $\Delta y = M\ p_y$ in height, to be reconstructed in a single operation. If the object is of a span ΔA_x greater than Δx the number of required horizontal scans is given by the spectral bandwidth ratio, which is to say :

$$n_x = \frac{\Delta\, u_{\text{objet}}}{\Delta\, u} = \left(\frac{\Delta\, A_x}{\lambda\, d_R}\right) / \left(\frac{\Delta\, x}{\lambda\, d_R}\right) = \frac{\Delta\, A_x}{N\ p_x}$$

It is simply equal to the sensor size/object size ratio. A similar relationship exists between the vertical scanning and n_y.

If the spectrum of the diffracted object wave is located at the frequential coordinates (u_0, v_0), the spatial frequencies of the filter bank are given in the two directions by :

$$\left(u_i\ ,\ v_i\right) = \left\{ u_0 + k_x \frac{N\ p_x}{\lambda\, d_R}\ ,\ v_0 + k_y \frac{M\ p_y}{\lambda\, d_R} \right\}$$

With

$$k_x \in \left\{ -\frac{n_x - 1}{2}\ ,\ +\frac{n_x - 1}{2} \right\} \qquad k_y \in \left\{ -\frac{n_y - 1}{2}\ ,\ +\frac{n_y - 1}{2} \right\}$$

The algorithm for spectral scanning is given in figure 18.

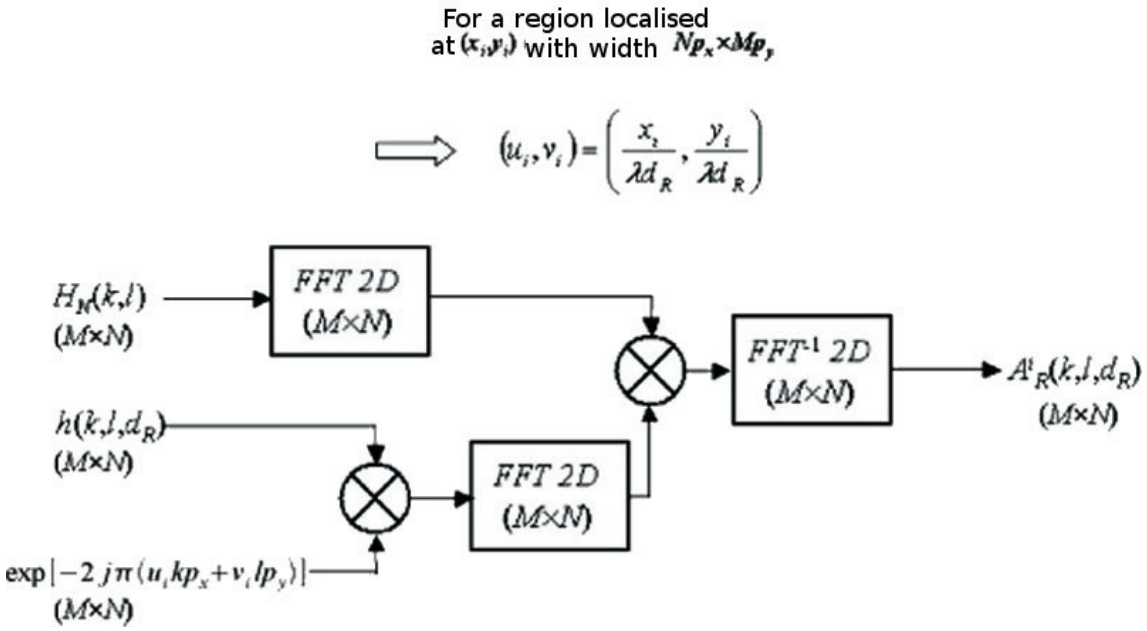

Figure 18 : Algorithm for spectral scanning

The form of the algorithm is the result of the properties of the Fourier transform regarding the spectral shift induced by the modulations in the direct space.

In order to reconstruct a region of the object whose central coordinated are (x_i, y_i) are and whose size is equal to that of the sensor $N\,p_x \times M\,p_y$, the central spatial frequency associated with that area is calculated ; that is to say $(u_i, v_i) = (x_i/\lambda d_R, y_i/\lambda d_R)$. The spectral filter associated with this area must therefore be focused on the coordinates in the spectrum of the hologram. The spectral alignment is thus carried out by modulation of the impulse response of the free space using numerical calculation :

$$h_i\left(k\,,l\,,d_R\right)=h\left(k\,,l\,,d_R\right)\times\exp\left(-2\,j\,\pi\left(u_i\,k\,p_x+v_i\,l\,p_y\right)\right)$$

Thus, the transfer function associated with the impulse response modulated by the spatial frequency in the spectral zone is :

$$\widetilde{H}_i\left(u\,,v\,,d_R\right)=\widetilde{H}\left(u-u_i\,,v-v_i\,,d_R\right)$$

With this transfer function, multiplied by the hologram spectrum, only the spectral zone of interest is kept. Thus, through spectral scanning by the filter bank method, the object can be reconstructed in its totality.

The larger the object in comparison to the size of the sensor, the more it is necessary to carry out the calculation using filters and the longer the reconstruction takes. In addition, the final image is obtained by the juxtaposition of adjacent reconstructed pieces: the size of the object image is now thus $n_y M \times n_x N$ pixels. If the number of scans imposes a final image size greater than 4096×4096pixels, the memory space being used will be considerable which will limit the possibilities for digital treatment of the obtained results.

j) Other strategies

Other reconstruction strategies exist which are based on the convolution equation. From the expression of the impulse responses and the associated transfer functions [[Introduction to Fourier Optics]], two other reconstruction methods can be distinguished :

- A filter bank derived from the exact form of $\widetilde{H}\left(u\,,v\,,d_R\right)$ with

$$\widetilde{H}\left(u\,,\,v\,,\,d_R\right)=\begin{cases}\exp\left(\dfrac{2\,j\,\pi\,d_R}{\lambda}\sqrt{1-\lambda^2\left(u^2+v^2\right)}\right) & \text{if} \quad u^2+v^2\le 1/\lambda^2\\ 0 \quad \text{elsewhere}\end{cases}$$

- A filter bank derived from the expression of $\widetilde{H}\left(u\,,v\,,d_R\right)$ in the Fresnel approximations with

$$\widetilde{H}\left(u\,,\,v\,,\,d_R\right)=\exp\left(\frac{2\,j\,\pi\,d_R}{\lambda}\right)\exp\left(-\,j\,\pi\,\lambda\,d_R\left(u^2+v^2\right)\right)$$

Taking into account the fact that spectral bands are finite in digital holography, these two expressions need to be adapted, firstly by limiting their spectral range and also by focusing their transfer function on $\left(u_i\,,v_i\right)$.

Thus they become respectively :

$$\widetilde{H}_i\left(u\,,\,v\,,\,d_R\right)=\begin{cases}\exp\left(\dfrac{2\,j\,\pi\,d_R}{\lambda}\sqrt{1-\lambda^2\left(\left(u-u_i\right)^2+\left(v-v_i\right)^2\right)}\right)\\ \quad \text{if} \quad \left|u-u_i\right|\le\dfrac{N\,p_x}{2\,\lambda\,d_R} \quad \text{and} \quad \left|v-v_i\right|\le\dfrac{M\,p_y}{2\,\lambda\,d_R}\\ 0 \quad \text{elsewhere}\end{cases}$$

And

$$\widetilde{H}_i\left(u\,,\,v\,,\,d_R\right)=\begin{cases}\exp\left(\dfrac{2\,j\,\pi\,d_R}{\lambda}\right)\exp\left(-\,j\,\pi\,\lambda\,d_R\left(\left(u-u_i\right)^2+\left(v-v_i\right)^2\right)\right)\\ \quad \text{if} \quad \left|u-u_i\right|\le\dfrac{N\,p_x}{2\,\lambda\,d_R} \quad \text{and} \quad \left|v-v_i\right|\le\dfrac{M\,p_y}{2\,\lambda\,d_R}\\ 0 \quad \text{elsewhere}\end{cases}$$

Figure 19 represents the reconstruction algorithm with the transfer functions.

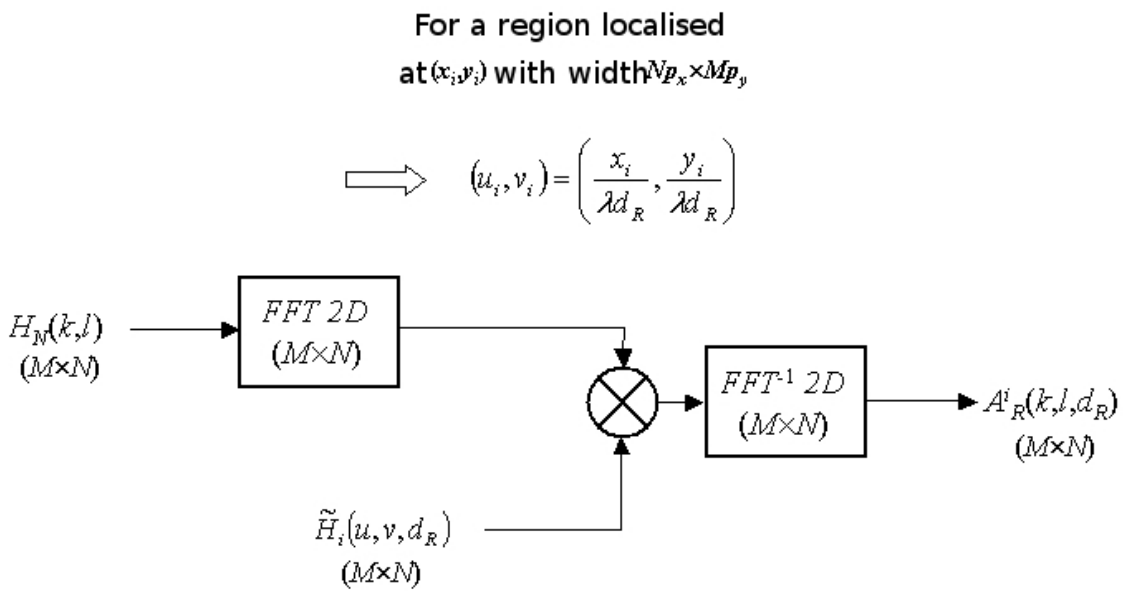

Figure 19 : Algorithm with the transfer functions

The method resembles that which was outlined in the previous paragraph and therefore the number of scans and the final image sizes are identical.

Methods of digital reconstruction by convolution are currently used in digital holographic microscopy : imaging using phase polarization or phase contrast [15 [Digital Holography for Quantitative Phase Contrast Imaging]] and also in 3D microscopy [16 [Image Formation in Phase Shifting Digital Holography and Application to Microscopy],17 [Short-Coherence Digital Microscopy by Use of a Lensless Holographic Imaging System]]. Indeed, reconstruction in different adjustment planes is only appropriate if the sampling pitch of the image remains constant.

* *

*

In this course, we have seen the different techniques and elements used for recording a hologram. We have established that in **"analogue" holography**, the principal of reconstructing the object wave front follows a "physical" approach, by using the recording laser.

As far as reconstruction by **digital holography** is concerned, it is necessary to correctly simulate the diffraction of the generally plane reference beam on the discretised hologram. In this case, the Fresnel transform can be implemented using direct or even by simulating a convolution.

Certain **approaches based on the use of wavelets** have been presented in other sources [18 [Diffraction From a Wavelet Point of View]] but have not been mentioned in this course.

Since the 1970s, "analogue" holography has been the object of a large number of studies which cover a large field of investigations: non-destructive control, study of fluids, study of particles, and live science . Research into holography is carried out notably for its use for non-contact and non-invasive measurement [19 [Holographic Interferometry]]. In this context, the research comprises comparison by interferometric channels of a hologram of an object said to be in a reference state with a hologram portraying its actual state. It seems that by this method it is possible to study structures which have been submitted to pneumatic, thermal or mechanic loadings in static, stationary or transitory conditions.

Holography allows for a global evaluation which is both qualitative, through the simple visualisation of the fringes which encode the displacement of the image and quantitative through the clearing of the fringes.

Over the last few years, Fresnel's "digital" holography has been much developed and has been used with some success in numerous fields. Indeed fascinating possibilities have been presented: imagery through a scattering medium [20 [Numerical Heterodyne Holography With Two-Dimensional Photodetector Arrays]], digital colour holography [21 [Phase Shifting Color Digital Holography]], the measurement of the surface outline [22 [Surface Shape Measurement by Phase Shifting Digital Holography]], the measurement of micro-composant parameters [23 [The Determination of Material Parameters of Microcomponents Using Digital Holography]], imagery by aperture synthesis [24 [Short-Range Synthetic Aperture Imaging at 633nm by Digital Holography]], suppression of the object aberrations [25 [Compensation of Lens Aberration in Digital Holography]], and the mechanical measurement of sptial-division multiplexing [26 [Twin Sensitivity Measurement by Spatial Multiplexing of Digitally Recorded Holograms]].

Digital holography is also a technology of the future which will be used in the comparison and the recognition of 3D objects as recent works on the subject has shown [28 [Three-Dimensional Object Recognition by Use of Digital Holography]] [29 [Comparative Digital Holography]].

III.Etude de cas

The point of this case study is to provide an example for the ideas found in the course on holography presenting experimental devices and images of holograms which have been digitally reconstructed using the Fresnel transform.

1. Digital holography device

The experimental device for recording the hologram is a Mach-Zehnder-type interferometer (figure 20).

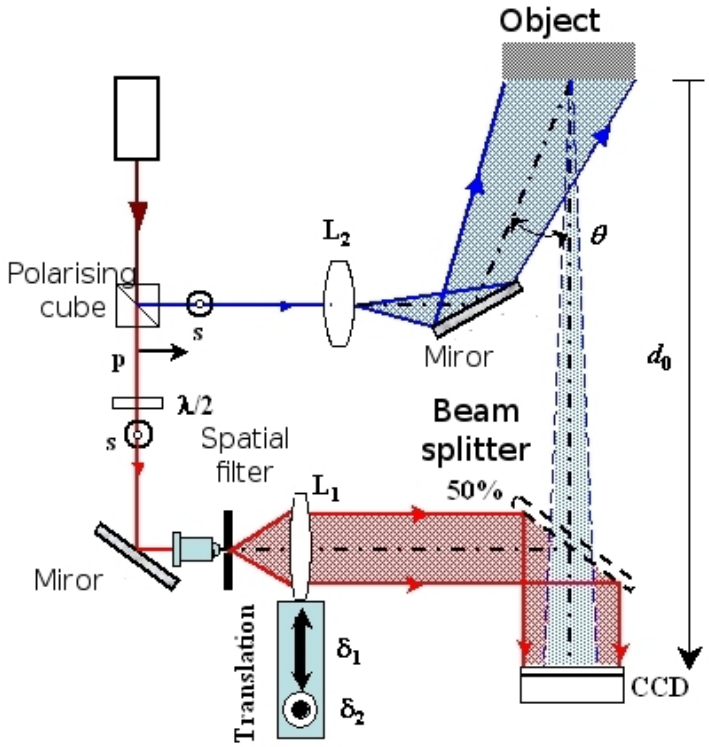

Figure 20 : Recording an off-axis digital hologram

The laser beam is split into two beams using beam splitter a cube. Thus, an object beam and a reference beam are obtained from the same monochromatic source. The half-wave plate placed at the laser source allows for the flux of the object and reference beams to be adjusted. The object beam is expanded by the lens L_2 so that it lights up the object . The angle of illumination of the object is adjusted by the rotation of a reflecting mirror . Then the object diffracts a wave towards the CCD-type sensor.

By this example, we can see that using digital holography it is only possible to record transmission holograms.

The reference beam is formed by a spatial filtering system: the beam is focused by a microscopic lens in a pinhole, the unwanted angular frequencies caused by slight deviation or energy distribution faults are gotten rid of. Thus, at the exit of the pinhole, we have a light source which is considered as 'pinpointed' giving a spherical wave form. The 'pinpointed' source is located at the focal phase from the convergent lens L_1 thus after crossing the lens, the reference beam is collimated. The system containing the spatial filter and the convergent lensL_1 constitutes the afocal system which allows a plane reference wave to be obtained. The reference wave is partially reflected onto the CCD sensor by the beam splitter (50%).

The reference wave and the object wave cause interference on the CCD plate. When the interferogram, which makes up the hologram, is generated in this way, it is discretised by the CCD sensor and then recorded. The sensor encodes the information using 12 bits which represents a dynamic of 4096 grey levels.

The lens L_1 allows for the collimation of the reference beam. This lens has another function which is to finely regulate the angular frequencies of the reference wave. Remember that according to the Shannon theory, the maximum incidence angle is 4. The lens L_1 is mounted on a micrometrical board. As figure 21 shows, the lens board can move in two directions: horizontally by δ_1 and vertically by δ_2. The aim of the vertical and horizontal movement of the lens is to tilt the reference wave at the angles θ_x and θ_y. Thus, the spatial frequencies of the reference wave are given by :

$$u_R = \frac{\sin(\theta_x)}{\lambda} = \frac{\delta_1 / f_1}{\lambda\sqrt{1+\delta_1^2/f_1^2}} \qquad v_R = \frac{\sin(\theta_y)}{\lambda} = \frac{\delta_2 / f_1}{\lambda\sqrt{1+\delta_2^2/f_1^2}}$$

Figure 21 illustrates the effect of the movement of the lens.

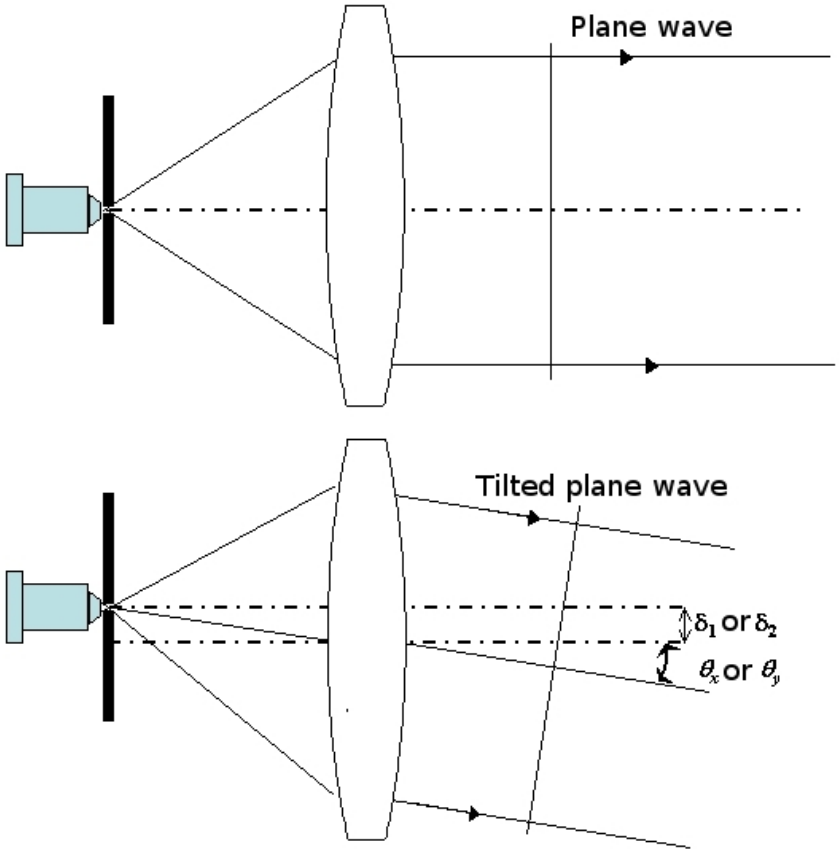

Figure 21 : Tilt of the reference wave

The CCD sensor contains $(M \times N) = (1024 \times 1360)$ pixels, each of a size $p_x = p_y = 4.65\mu\ \mathrm{m}$.

The object if a 2 euro coin placed at a distance of $d_0 = 660\ \mathrm{mm}$ from the sensor. The spatial frequencies are adjusted to $u_R = -71.8\ \mathrm{mm}^{-1}$ and $v_R = -62.65\ \mathrm{mm}^{-1}$.

2. The digitally reconstructed hologram

The hologram of the object, recorded by the CCD sensor is shown in figure 22. The recorded image has an unpredictable character which is given to it by the speckle field produced by the wave diffracted by the object.

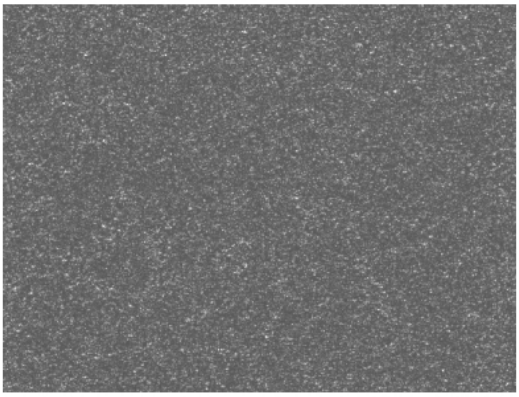

Figure 22 : Digitally recorded hologram

When $d_R = -660\ \text{mm}$ is chosen as the algorithm for reconstruction using the direct Fresnel transform, the digital focusing of the object is in the $+1$-order. The amplitude of the field numerically diffracted using $K = L = 2048$ points is shown in figure 23.

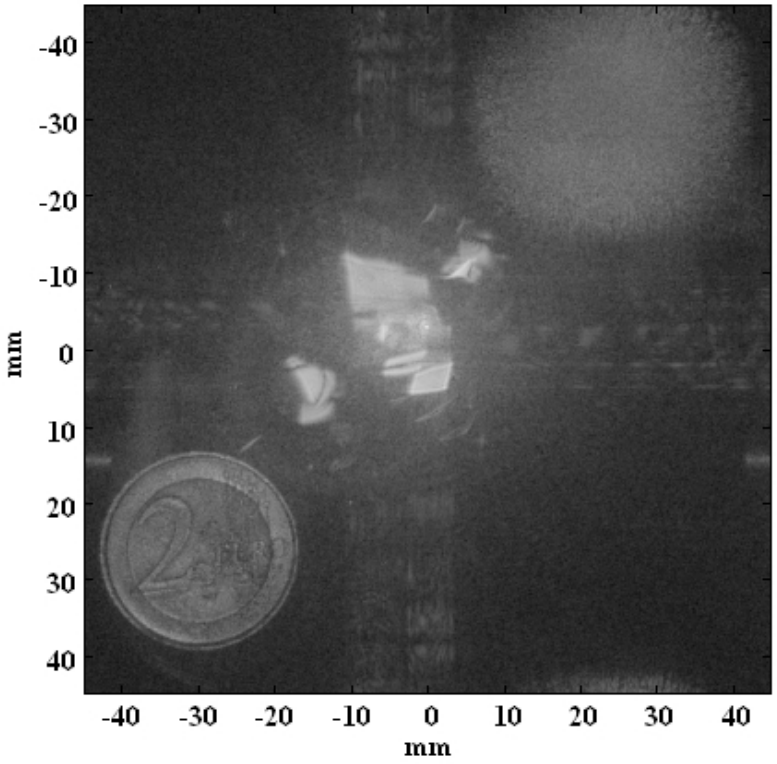

Figure 23 : The diffracted field when dR = -660 nm

The image resolution is $R_x = 66.0\ \mu\text{m}$ and $R_x = 87.7\ \mu\text{m}$ and the sampling pitch is $\Delta\xi = \Delta\eta = 43.85\mu\ \text{m}$. The Reconstructed field covers an area of $90.63 \times 90.63\ \text{mm}^{-2}$. Taking into account the theoretical elements presented in this course, the $+1$-order is located at the coordinates $(x_0, y_0) \approx (-30\ \text{mm} + 26.2\ \text{mm})$ which correspond to the pixel coordinates $(u_R K p_x, v_R L p_y) \approx (-683, +596)$.

When, $d_R = +660\ \text{mm}$ is imposed, focusing is in the -1-order, the calculated fields having the same area as before. This is illustrated in figure 24.

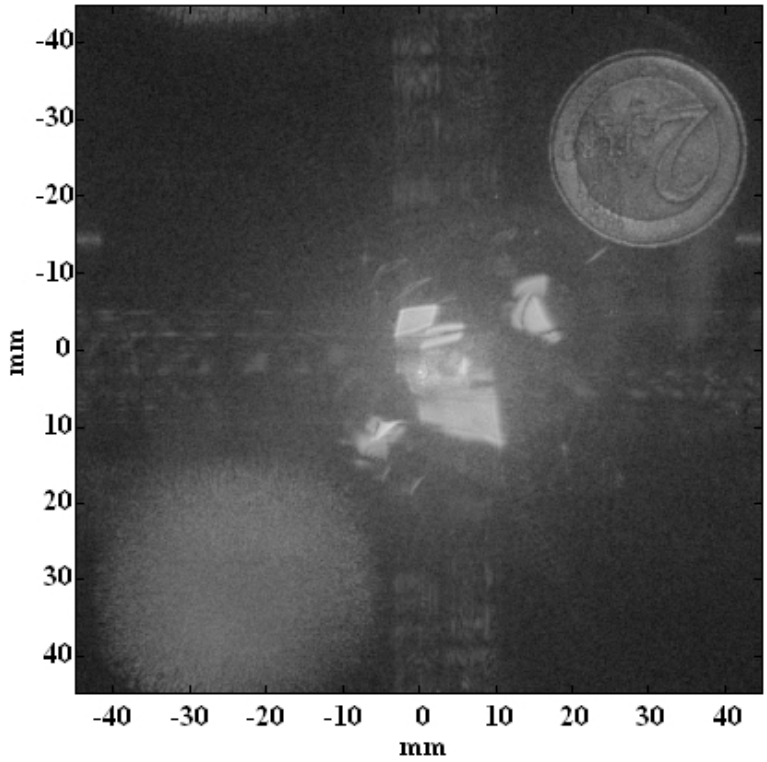

Figure 24 : The diffracted field when dR = +660 mm

Taking in to account the hermitian symmetric properties of the Fourier transform, the -1-order is flipped and located at the coordinates $(x_0, y_0) \approx (+30\ \text{mm}, -26.2\ \text{mm})$, which correspond to the pixel coordinates $(u_R K p_x, v_R L p_y) \approx (+683, -596)$.

If a reconstruction distance other than $|d_0|$, is chosen, the image will be blurred.

The animation shown in figure 25 illustrates the formation of the image based on the distance imposed by the algorithm of the Fresnel transform.

3. The effect of zero-padding

It was mentioned in the course material that it is possible to carry out a 'zero-padding' and what the consequences of this are. This aspect is represented in figure 26 which shows the area round the "2" on the coin as it appears for reconstruction with a varying number of points $(512, 1024, 2048, 4096)$.

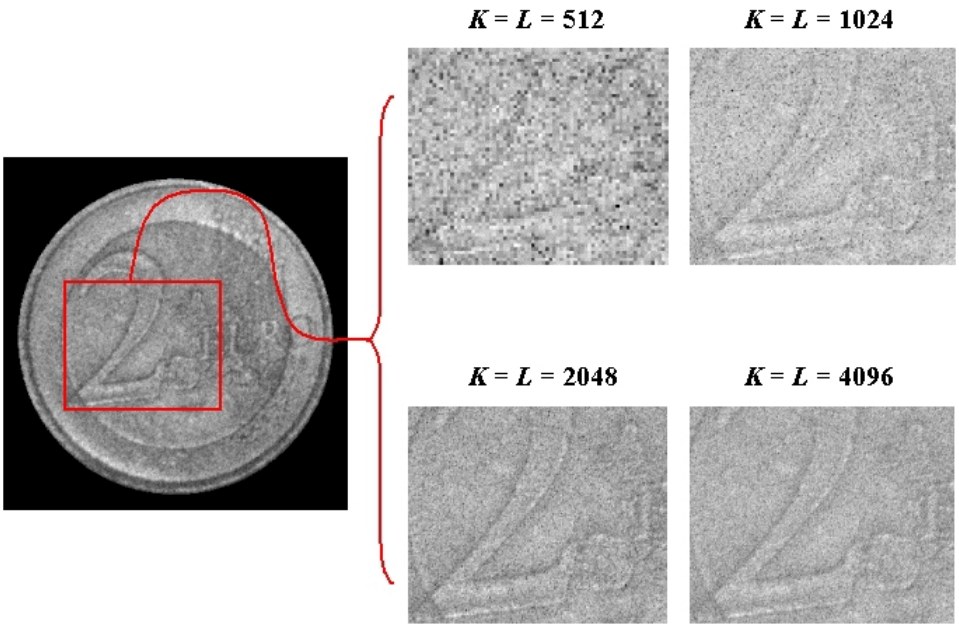

Figure 26 : Effect of zero-padding

When $K = L = 512$, the hologram is truncated since the number of points which have been retained is a lot lower than the initial matrix (1024×1360). In this case, the resolution is reduced because $R_x = R_y = \Delta\xi = \Delta\eta = 175.42\mu\,\mathrm{m}$; the reconstructed image appears badly formed. When $K = L = 1024$, the number of points that have been retained is roughly equal to that provided by the sensor (1024 against 1360 horizontally); the image sampling corresponds to the intrinsic resolution given by the pixel matrix, which is $R_x = R_y = \Delta\xi = \Delta\eta = 87.7\mu\,\mathrm{m}$; therefore the image appears to be "pixelised".

For $K = L = 2048$, zero-padding is effective and the sampling of the image plane is half the resolution; the resolution function $\tilde{W}_{NM}$ is therefore sampled with the better definition which allow for the fine texture of the image and in particular its speckle granularity to be brought into perspective. For $K = L = 4096$, the sampling of the image plane is now four times smaller than the resolution. We get $R_x = 66.0\mu\,\mathrm{m}$ and $R_y = 87.7\mu\,\mathrm{m}$ and the sampling pitch is $\Delta\xi = \Delta\eta = 21.92\mu\,\mathrm{m}$. The definition of the image plane is even better but the speckle granularity doesn't necessarily change with size; it is imposed by the resolution of the method and therefore by the size of the CCD sensor.

4. Reconstruction by convolution

The hologram in figure 22 was used to illustrate reconstruction by convolution.

The pixel matrix covers an area of $(Np_x \times Mp_y) = (6.32 \times 4.76)\ \mathrm{mm}$. The object has a diameter of $25\ \mathrm{mm}$; the number of spectral scans is therefore $(n_x, n_y) = (4, 6)$ and the reconstructed field made by the attachment of the different zones would contain $(L \times K) = (6144 \times 5440)$ pixels, which is a considerable size! The sampling pitch of the reconstructed field is the same as that for the sensor $\Delta\xi = \Delta\eta = 4.65\mu\,\mathrm{m}$.

The spectral contents of the hologram is given by its Fourier transform. Taking into account the modelling we saw in the course for the plane reference wave, we get :

$$\begin{aligned}\widetilde{E}(u\,,\,v) &= \mathrm{TF}\left[H\left(x\,,\,y\,,\,d_0\right)\right](u\,,\,v)\\ &= \widetilde{O}_0(u\,,\,v) + \widetilde{O}\left(u - u_R\,,\,v - v_R\right) + \widetilde{O}^*\left(u + u_R\,,\,v + v_R\right) + a_R^2\,\delta(u\,,\,v)\end{aligned}$$

Where $\tilde{O}(u,v)$ is the Fourier transform of the wave diffracted by the object and $\tilde{O}_0(u,v)$ is the Fourier transform of $|O|^2$. The spectrum is therefore trimodal and the spectral content which corresponds to the object is located at the frequential coordinates (u_R, v_R).The filter bank used in the reconstruction of the object must therefore scan the spectral zone which surrounds the average frequency $(u_R; v_R) = (-71.8\ \text{mm}^{-1}\ ; -62.65\ \text{mm}^{-1})$.

Figure 27 shows the hologram's spectrum.

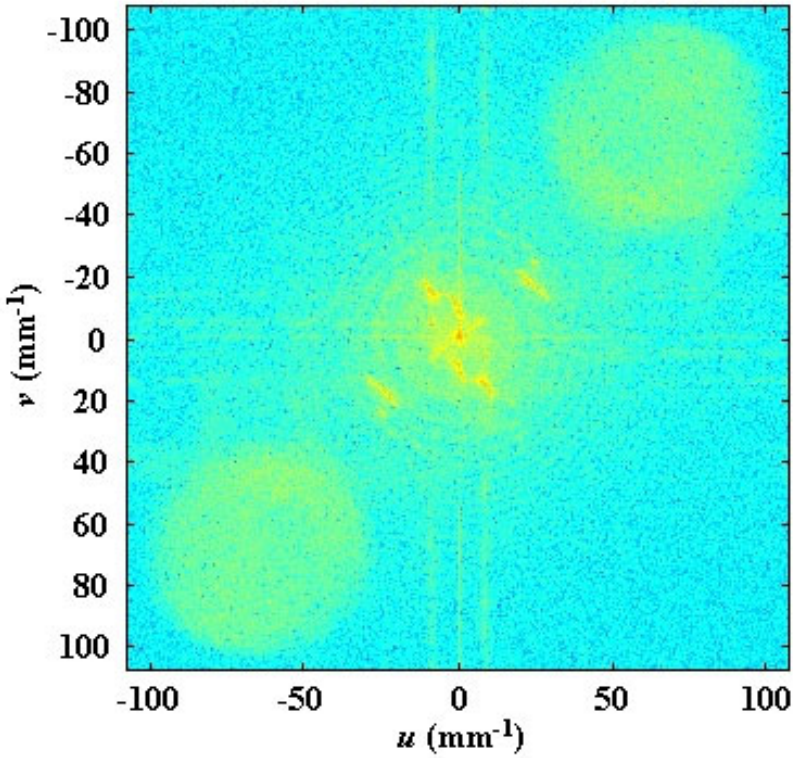

Figure 27 : The hologram's spectrum

Figure 28 shows the spectrum of the exact impulse response of the free space which is used in reconstruction by convolution.

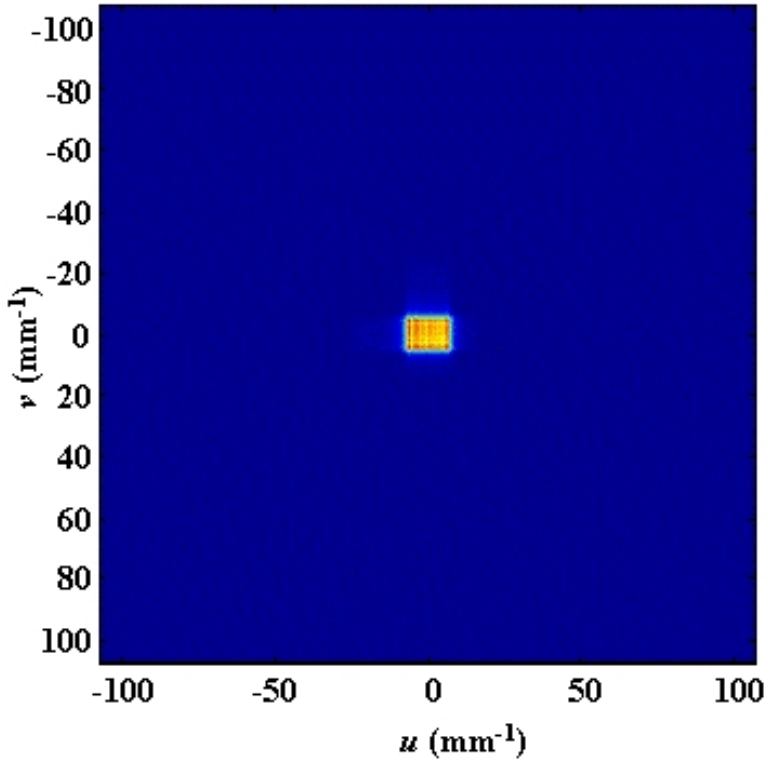

Figure 28 : Spectrum of the transfer function of the free space

The bandwidth of the transfer function of the free space is clearly insufficient in order to cover the useful bandwidth of the hologram in a single operation.

Figure 29 shows the $+1$-order reconstructed by convolution by applying the algorithm shown in figure 18.

Figure 29 : Hologram reconstructed by convolution

Figure 30 shows a comparison between the object reconstructed by 4096 point zero-padding and the object reconstructed by convolution.

Figure 30 : Hologram reconstructed by convolution

We can see that the convolution gives a result which corresponds to that given by zero-padding with a format which does not match the number of points required for FFT algorithms (in 2n).

Remarque

The convolution method is highly appropriate for use with small objects but on the other hand is not recommended for objects which are larger than the pixel matrix because the final image contains a considerable number of points which increase the necessary calculation time and makes any digital processing highly delicate.

IV.Exercice

The part of the course which deals with analogue holography outlines the process of image formation when the laser beam used for reconstruction is identical to that used for the recording. We saw that the reconstructed object is identical to the recorded one.

However, in practical situations it is often the case that the recording beam is not used for the reconstruction. Thus, the reference wave length and wave front are different than the recording wave length and wave front. Because of the properties of holograms and of diffraction, the object is visible but with a different location and size than the initial object. The exercise section will discuss this point and we will attempt to outline the interconnected relationships of holography.

1. Auto-corrective exercises

Preliminaries

The geometry is shown in figure 31 ; the set of reference coordinates is that of the hologram.

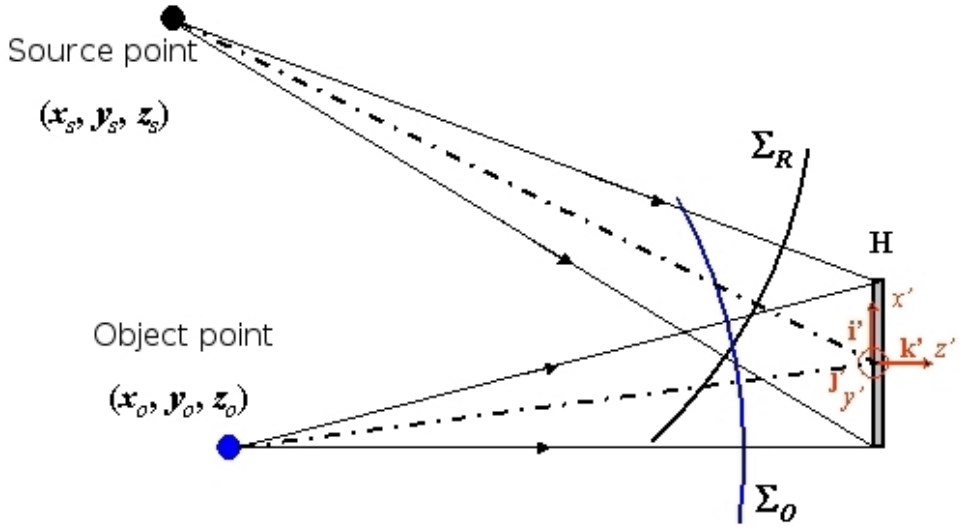

Figure 31 : Geometry for the recording

We consider that the source pinhole is finely localised, with wavelength λ, located at (x_s, y_s, z_s), and it emits a divergent spherical wave towards the holographic plane. The object would be considered as being local and would be located at (x_0, y_0, z_0).

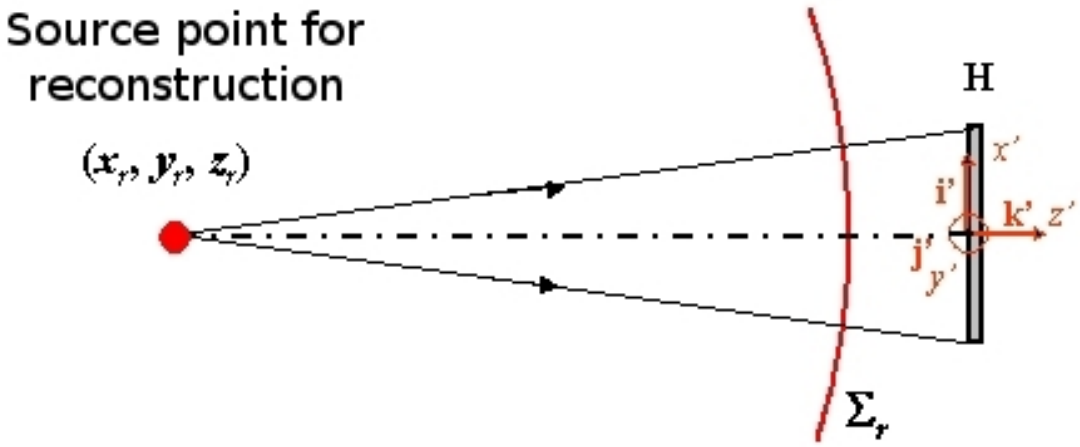

Figure 32 : Geometry for the reconstruction

For the physical reconstruction process, we consider that the source pinhole which provides the illumination of the hologram is located at $(x_r, y_r, z_r)$and that its wave length is λ_r, with $\lambda_r \neq \lambda$.

Question 1

[*Solution n°1 p 45*]

Question 1 : Express the total complex amplitude in the holographic plane during the recoding. From that, deduce the expression of the hologram.

Question 2

[*Solution n°2 p 45*]

Question 2 : Express the transmittance of the hologram for the $+1$-order and for the -1-order.

Question 3

[*Solution n°3 p 46*]

Question 3 : Express the complex amplitude which comes from the reconstruction wave and which is incident in the holographic plane. From that deduct the expression of the transmitted waves in the $+1$ and -1-orders.

Question 4

[*Solution n°4 p 46*]

Question 4 : From the previous result, deduct that the waves in both the $+1$ and -1-orders are spherical waves of wave length λ_r emanating from an image point with the coordinates (x_i, y_i, z_i). From that, deduct the expression of (x_i, y_i, z_i), in each order for λ_r, λ, (x_s, y_s, z_s), (x_o, y_o, z_o) and (x_r, y_r, z_r).

Question 5

[*Solution n°5 p 48*]

Question 5 : From the expressions of the coordinates of the source point; work out the axial magnification g_z and the transverse magnification g_x et g_y, for the object-image relationship in the $+1$-order.

Question 6

[*Solution n°6 p 49*]

Question 6 : Numerical application: an object is recorded situated at $(0, 0, -70\ \text{cm})$ with a helium-neon laser coming from the source pinhole located at $(40\ \text{cm}, 0, -100\ \text{cm})$. The reconstruction is carried out with a duplicated NdYAG laser coming from the source pinhole located at $(-30\ \text{cm}, 0, -80\ \text{cm})$.

From this deduct the position of the image and the ratio of the object and image sizes.

Solution des exercices

>Solution n°1 *(exercice p. 44)*

Taking into account the notations given in the course, (z_s, z_0) being negative in figure 31, the reference wave front is written :

$$R(x',y') = a_R \exp\left(-\frac{j\pi}{\lambda z_s}\left[(x'-x_s)^2+(y'-y_s)^2\right]\right)$$

The object wave front is written :

$$O(x',y') = a_O \exp\left(-\frac{j\pi}{\lambda z_o}\left[(x'-x_o)^2+(y'-y_o)^2\right]\right)$$

The total field is equal to the sum of the amplitudes, that is to say :

$$U(x',y') = a_R \exp\left(-\frac{j\pi}{\lambda z_s}\left[(x'-x_s)^2+(y'-y_s)^2\right]\right) + a_O \exp\left(-\frac{j\pi}{\lambda z_o}\left[(x'-x_o)^2+(y'-y_o)^2\right]\right)$$

From this it is possible to deduct the expression of the hologram since $H(x',y') = |U(x',y')|^2$:

$$H(x',y') = a_R^2 + a_O^2 + a_R a_O \exp\left(-\frac{j\pi}{\lambda z_s}\left[(x'-x_s)^2+(y'-y_s)^2\right]+\frac{j\pi}{\lambda z_o}\left[(x'-x_o)^2+(y'-y_o)^2\right]\right)$$
$$+ a_R a_O \exp\left(+\frac{j\pi}{\lambda z_s}\left[(x'-x_s)^2+(y'-y_s)^2\right]-\frac{j\pi}{\lambda z_o}\left[(x'-x_o)^2+(y'-y_o)^2\right]\right)$$

>Solution n°2 *(exercice p. 44)*

Taking into account that :

$$t = t_0 - \beta \Delta t \left(R^* O + R O^*\right)$$

Where Δt is the exposure time and β is the sensitivity of the recording plate, we get the transmission in the $+1$-order as :

$$t_{+1} = -\beta \Delta t R^* O$$
$$= -\beta \Delta t a_R a_O \exp\left(+\frac{j\pi}{\lambda z_s}\left[(x'-x_s)^2+(y'-y_s)^2\right]-\frac{j\pi}{\lambda z_o}\left[(x'-x_o)^2+(y'-y_o)^2\right]\right)$$

And the transmission in the -1-order as :

$$t_{-1} = -\beta \Delta t R O^*$$
$$= -\beta \Delta t a_R a_O \exp\left(-\frac{j\pi}{\lambda z_s}\left[(x'-x_s)^2+(y'-y_s)^2\right]+\frac{j\pi}{\lambda z_o}\left[(x'-x_o)^2+(y'-y_o)^2\right]\right)$$

>Solution n°3 *(exercice p. 44)*

Taking into account what we have seen above, we get the following expression for the reconstruction wave :

$$R_r(x',y') = a_r \exp\left(-\frac{j\pi}{\lambda_r z_r}\left[(x'-x_r)^2+(y'-y_r)^2\right]\right)$$

In the $+1$-order, the transmitted wave is :

$$\begin{aligned} A_R^{+1} &= R_r t_{+1} \\ &= -\beta \Delta t\, R^*\, O\, R_r \end{aligned}$$

That is to say :

$$\begin{aligned} &A_R^{+1}(x',y') \\ &= -\beta \Delta t\, a_R\, a_O\, a_r \exp\left(+\frac{j\pi}{\lambda z_s}\left[(x'-x_s)^2+(y'-y_s)^2\right]-\frac{j\pi}{\lambda z_o}\left[(x'-x_o)^2+(y'-y_o)^2\right]-\frac{j\pi}{\lambda_r z_r}\left[(x'-x_r)^2+(y'-y_r)^2\right]\right) \end{aligned}$$

In the -1-order, the transmitted wave is :

$$\begin{aligned} A_R^{-1} &= R_r t_{-1} \\ &= -\beta \Delta t\, R\, O^*\, R_r \end{aligned}$$

That is to say :

$$\begin{aligned} &A_R^{-1}(x',y') \\ &= -\beta \Delta t\, a_R\, a_O\, a_r \exp\left(-\frac{j\pi}{\lambda z_s}\left[(x'-x_s)^2+(y'-y_s)^2\right]+\frac{j\pi}{\lambda z_o}\left[(x'-x_o)^2+(y'-y_o)^2\right]-\frac{j\pi}{\lambda_r z_r}\left[(x'-x_r)^2+(y'-y_r)^2\right]\right) \end{aligned}$$

>Solution n°4 *(exercice p. 44)*

According to the results of question 3, the emerging wave is obtained by the product of the spherical reference, object and reconstruction wavelets. It is therefore possible to deduct from this that the emerging wave is also a wave with the same characteristics.

For the $+1$-order, since the image point should be virtual and the wave front divergent, we get the expression :

$$A_R^{+1}(x',y') = a_R^{+1} \exp\left(-\frac{j\pi}{\lambda_r z_i}\left[(x'-x_i)^2+(y'-y_i)^2\right]\right)$$

And for the -1-order, since the image point should be real and the wave front convergent, we get :

$$A_R^{+1}(x',y') = a_R^{-1} \exp\left(\frac{j\pi}{\lambda_r z_i}\left[(x'-x_i)^2+(y'-y_i)^2\right]\right)$$

By developing the quadratic terms of the complex exponentials and by assimilating them with the expression retained for A_R^{+1} and A_R^{+1}, we get :

- for the coefficients of the terms in (x'^2, y'^2) in the $+1$**-order** :

$$-\frac{\pi}{\lambda_r z_i} = +\frac{\pi}{\lambda z_s} - \frac{\pi}{\lambda z_o} - \frac{\pi}{\lambda_r z_r}$$

Giving the axial position of the source point from which the diffracted wave emanates,

$$\frac{1}{z_i} = -\frac{\lambda_r}{\lambda z_s} + \frac{\lambda_r}{\lambda z_o} + \frac{1}{z_r}$$

- For the coefficients of the terms in (x'^2, y'^2) in the -1**-order** :

$$\frac{\pi}{\lambda_r z_i} = -\frac{\pi}{\lambda z_s} + \frac{\pi}{\lambda z_o} - \frac{\pi}{\lambda_r z_r}$$

Giving the axial position of the source point from which the diffracted wave emanates,

$$\frac{1}{z_i} = -\frac{\lambda_r}{\lambda z_s} + \frac{\lambda_r}{\lambda z_o} - \frac{1}{z_r}$$

- For the coefficients of the terms in (x', y') in the $+1$**-order** :

$$-\frac{\pi x_i}{\lambda_r z_i} = +\frac{\pi x_s}{\lambda z_s} - \frac{\pi x_o}{\lambda z_o} - \frac{\pi x_r}{\lambda_r z_r}$$
$$-\frac{\pi y_i}{\lambda_r z_i} = +\frac{\pi y_s}{\lambda z_s} - \frac{\pi y_o}{\lambda z_o} - \frac{\pi y_r}{\lambda_r z_r}$$

The coordinates (x_i, y_i) of the source point from which the diffracted wave emanates are :

$$x_i = -\frac{x_s \lambda_r z_i}{\lambda z_s} + \frac{x_o \lambda_r z_i}{\lambda z_o} + \frac{x_r z_i}{z_r}$$
$$y_i = -\frac{y_s \lambda_r z_i}{\lambda z_s} + \frac{y_o \lambda_r z_i}{\lambda z_o} + \frac{y_r z_i}{z_r}$$

- For the coefficients of the terms in (x', y') in the -1**-order** :

$$\frac{\pi x_i}{\lambda_r z_i} = -\frac{\pi x_s}{\lambda z_s} + \frac{\pi x_o}{\lambda z_o} - \frac{\pi x_r}{\lambda_r z_r}$$
$$\frac{\pi y_i}{\lambda_r z_i} = -\frac{\pi y_s}{\lambda z_s} + \frac{\pi y_o}{\lambda z_o} - \frac{\pi y_r}{\lambda_r z_r}$$

The coordinates (x_i, y_i) of the source point from which the diffracted wave emanates are :

$$x_i = -\frac{x_s \lambda_r z_i}{\lambda z_s} + \frac{x_o \lambda_r z_i}{\lambda z_o} - \frac{x_r z_i}{z_r}$$
$$y_i = -\frac{y_s \lambda_r z_i}{\lambda z_s} + \frac{y_o \lambda_r z_i}{\lambda z_o} - \frac{y_r z_i}{z_r}$$

>Solution n°5 *(exercice p. 44)*

For any variation of the position of the object, we see a variation of the position of the image point ; thus we get :

$$g_x = \frac{\partial x_i}{\partial x_o} \qquad g_y = \frac{\partial y_i}{\partial y_o} \qquad g_z = \frac{\partial z_i}{\partial z_o}$$

It can be deduced from this and the previous expressions that :

$$g_x = \frac{\partial x_i}{\partial x_o} = g_y = \frac{\partial y_i}{\partial y_o} = \frac{\lambda_r z_i}{\lambda z_o}$$

For the axial magnification :

$$g_z = \frac{\partial}{\partial z_o}\left(-\frac{\lambda_r}{\lambda z_s} + \frac{\lambda_r}{\lambda z_o} + \frac{1}{z_r}\right)^{-1}$$

The calculation gives :

$$g_z = \frac{\lambda_r}{\lambda}\frac{z_i^2}{z_o^2}$$

Which can also be written :

$$g_z = \frac{\lambda}{\lambda_r} g_x^2$$

We find a classic result of geometric optics where the axial magnification is proportional to the square of the trasverse one.

>Solution n°6 *(exercice p. 44)*

The geometry of the recording is shown in figure 33 :

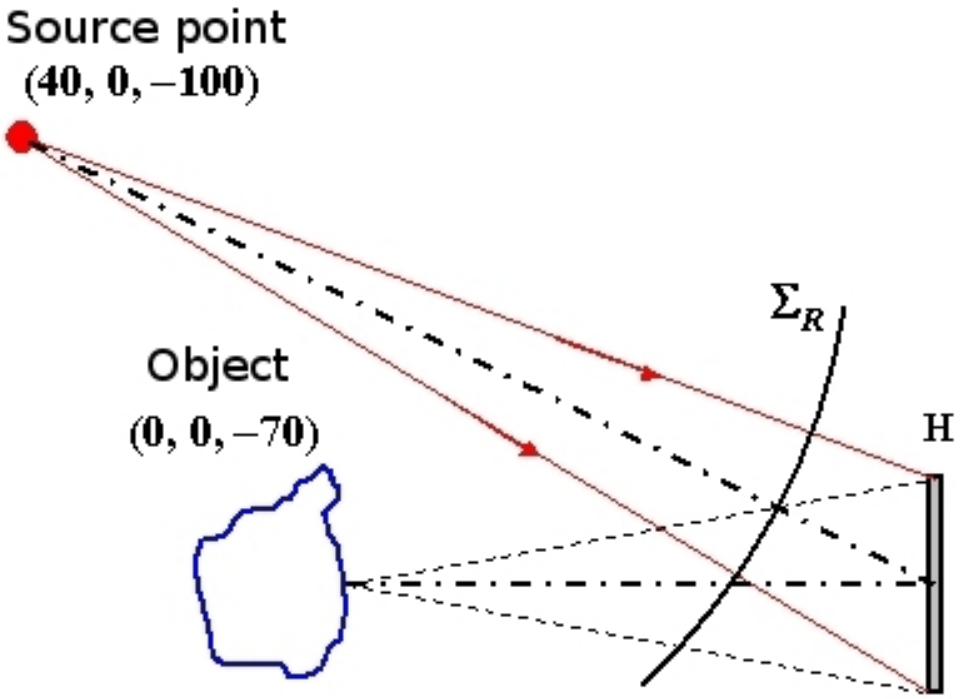

Figure 33 : Geometry of the recording

$$z_i = \left(-\frac{532}{632,8 \times (-100)} + \frac{532}{632,8 \times (-70)} + \frac{1}{-80} \right)^{-1} = -61,10 \text{ cm}$$

The transverse positions are :

$$x_i = -\frac{x_s \lambda_r z_i}{\lambda z_s} + \frac{x_o \lambda_r z_i}{\lambda z_o} + \frac{x_r z_i}{z_r} = -\frac{40 \times 532 \times (-61,1)}{632,8 \times (-100)} + \frac{0 \times 532 \times (-61,1)}{632,8 \times (-70)} + \frac{(-30) \times (-61,1)}{-80}$$

That is to say $x_i = -44.17$ cm and $y_i = 0$ cm.
The transverse magnification is :

$$g_x = \frac{\lambda_r z_i}{\lambda z_o} = \frac{532 \times (-61,1)}{632,8 \times (-70)} = 0,745$$

The reconstructed object is therefore closer to the hologram and almost 25% smaller than the real object. It is located to the left of the real object.

Figure 34 represents the reconstuction of the virtual image :

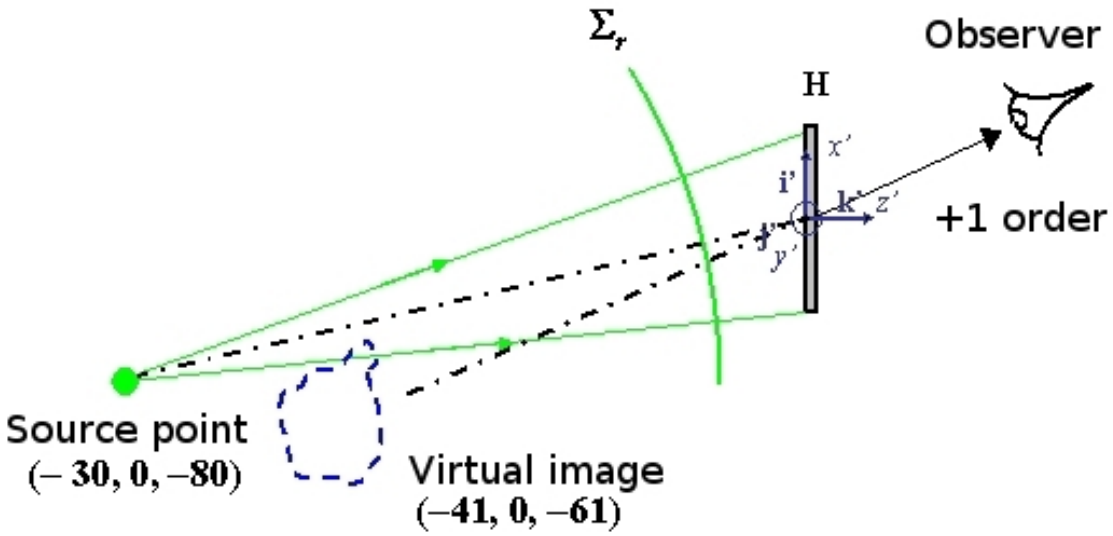

Figure 34 : Reconstructed virtual image

Bibliographie

[A New Microscopic Principle] Gabor D., *A New Microscopic Principle* (p.pp 777-778), Nature, 1948--, n° Vol. 161, .

[A Quarter Century of Thermoplastic Holography] Parker R.J., *A Quarter Century of Thermoplastic Holography* (p.224-271), International Conference on Hologram Interferometry and Speckle Metrology, *K. Stetson, R. Pryputniewiscz (1990)*, .

[Comparative Digital Holography] Osten W., Baumbach T., Juptner W., *Comparative Digital Holography* (p.pp 1764-1766), Optics Letters, 2002--, Vol. 27, n° N°20, .

[Compensation of Lens Aberration in Digital Holography] Stadelmaier A., Massig J.H., *Compensation of Lens Aberration in Digital Holography* (p.pp 1630-1632), Optics Letters, 2000--, Vol. 25, n° N°22, .

[Diffraction From a Wavelet Point of View] Onural L., *Diffraction From a Wavelet Point of View* (p.pp 846-848), Optics Letters, 1993--, Vol. 18, n° N°11, .

[Digital Holography for Quantitative Phase Contrast Imaging] Cuche E., Bevilacqua F., Depeursinge C., *Digital Holography for Quantitative Phase Contrast Imaging* (p.pp 291-293), Optics Letters, 1999--, Vol. 24, n° N°5, .

[Direct Recording of Holograms by a CCD Target and Numerical Reconstruction] Schnars U., Jüptner W., *Direct Recording of Holograms by a CCD Target and Numerical Reconstruction* (p.pp 179-181), Applied Optics, 1994--, Vol. 33, n° N°2, .

[Holographic Interferometry] West C.M., *Holographic Interferometry*, John Wiley & Sons, New York, 1979.

[Holographic Interferometry – Principles and Methods] Kreis Thomas, *Holographic Interferometry – Principles and Methods*, Akademie Verlag, Berlin, 1996.

[Holographie Industrielle] Smigielski Paul, *Holographie Industrielle*, Teknéa, Toulouse, 1994.

[Image Formation in Phase Shifting Digital Holography and Application to Microscopy] Yamaguchi I., Kato J., Ohta S., Mizuno J., *Image Formation in Phase Shifting Digital Holography and Application to Microscopy* (p.pp 6177-6186), Applied Optics, 2001--, Vol. 40, n° N°34, .

[Introduction to Fourier Optics] Goodman Joseph, *Introduction to Fourier Optics*, McGraw-Hill, New York, 1996.

[Methods of Digital Holography : a Comparison] Kreis Th., Adams M., Jüptner W., *Methods of Digital Holography : a Comparison* (p.Vol. 3098), Proceedings SPIE (1997) éditeur: C. Gorecki, *Optical Inspection and Micromeasurements II*, .

[Numerical Heterodyne Holography With Two-Dimensional Photodetector Arrays] Le Clerc F., Collot L., Gross M., *Numerical Heterodyne Holography With Two-Dimensional Photodetector Arrays* (p.pp 716-718), Optics Letters, 2000--, Vol. 25, n° N°10, .

[Phase Shifting Color Digital Holography] Yamaguchi I., Matsumura T., Kato J., *Phase Shifting Color Digital Holography* (p.pp 1108-1110), Optics Letters, 2002--, Vol. 27, n° N°13, .

[Phase Shifting Digital Holography] Yamaguchi I., Zhang T., *Phase Shifting Digital Holography* (p.pp 1268-1270), Optics Letters, 1997--, Vol. 22, n° N°16, .

[Photographic Reconstruction of the Optical Properties of an Object in its Own Scattered Radiation Field] Denisyuk Y.N., *Photographic Reconstruction of the Optical Properties of an Object in its Own Scattered Radiation Field* (p.pp 1275-1279), Doklady Academii Nauk SSSR, 1962--, n° Vol. 144, .

[Real Time Metrology With BSO Cristals] Tiziani H.J., *Real Time Metrology With BSO Cristals* (p.pp 463-470), Optica Acta, 1982--, n° Vol. 29, .

[Reconstructed Wavefront and Communication Theory] Leith E.N., Upatnieks J., *Reconstructed Wavefront and Communication Theory*, Journal of the Optical Society of America, 1962--.

[Reconstruction of a Hologram With a Computer] Kronrod M.A., Merzlyakov N.S., Yaroslavskii L.P., *Reconstruction of a Hologram With a Computer* (p.pp 333-334), Soviet Physics Technical Physics, 1972--, n° Vol. 17, .

[Short-Coherence Digital Microscopy by Use of a Lensless Holographic Imaging System] Pedrini G., Tiziani H.J., *Short-Coherence Digital Microscopy by Use of a Lensless Holographic Imaging System* (p.pp 4489-4496), Applied Optics, 2002--, Vol. 41, n° N°22, .

[Short-Range Synthetic Aperture Imaging at 633nm by Digital Holography] Binet R., Colineau J., Lehureau J.C., *Short-Range Synthetic Aperture Imaging at 633nm by Digital Holography* (p.pp 4775-4782), Applied Optics, 2002--, Vol. 41, n° N°23, .

[Surface Shape Measurement by Phase Shifting Digital Holography] Yamaguchi I., Kato J., Ohta S., *Surface Shape Measurement by Phase Shifting Digital Holography* (p.pp 85-89), Optical Review, 2001--, Vol. 8, n° N°2, .

[The Determination of Material Parameters of Microcomponents Using Digital Holography] Seebacher S., Osten W., Baumbach, T., Juptner W., *The Determination of Material Parameters of Microcomponents Using Digital Holography* (p.pp 103-126), Optics and Lasers in Engineering, 2001--, Vol. 36, n° N°2, .

[Three-Dimensional Object Recognition by Use of Digital Holography] Javidi B., Tajahuerce E., *Three-Dimensional Object Recognition by Use of Digital Holography* (p.pp 610-612), Optics Letters, 2000--, Vol. 25, n° N°9, .

[Twin Sensitivity Measurement by Spatial Multiplexing of Digitally Recorded Holograms] Picart P., Moisson E., Mounier D., *Twin Sensitivity Measurement by Spatial Multiplexing of Digitally Recorded Holograms* (p.pp 1947-1957), Applied Optics, 2003--, Vol. 42, n° N°11, .

[Wavefront Reconstruction With Diffused Illumination and Three-Dimensional Objects] Leith E.N., Upatnieks J., *Wavefront Reconstruction With Diffused Illumination and Three-Dimensional Objects* (p.pp 1295-130), Journal of the Optical Society of America, 1964--, Vol. 54, n° N°11, .

Webographie

[] *http:/www.optrion-tech.com* (consultation - - 2006).